

AD-A186 726

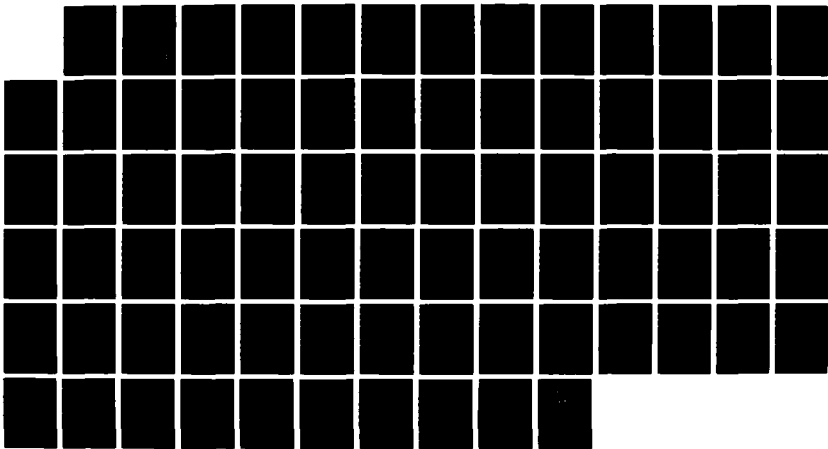
RADIANT POWER DEGRADATION OF SILICON-DOPED GALLIUM  
ARSENIDE AND GALLIUM A. (U) AIR FORCE INST OF TECH  
WRIGHT-PATTERSON AFB OH W N RESINONT MAY 87  
AFIT/CI/NR-87-677

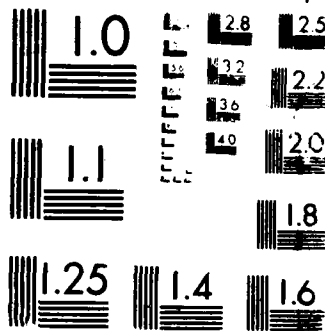
1/1

UNCLASSIFIED

F/G 28/12

ML





MICROSCOPY RESOLUTION TEST CHART  
NATIONAL BUREAU OF STANDARDS-1963-A

AD-A186 726

①

RADIANT POWER DEGRADATION OF SILICON-DOPED GALLIUM  
ARSENIDE AND GALLIUM ALUMINUM ARSENIDE INFRARED  
LIGHT-EMITTING DIODES

DTIC FILE COPY

A thesis submitted in partial fulfillment  
of the requirements for the degree of  
Master of Science

By

WILLIAM NORDIN RESIMONT, B.S.E.E.  
University of Arkansas, 1985

May 1987  
University of Arkansas

DTIC  
ELECTE  
OCT 27 1987  
S D  
u H

DISTRIBUTION STATEMENT A

Approved for public release;  
Distribution Unlimited

87 10 14 251

REPORT DOCUMENTATION PAGE		READ INSTRUCTIONS BEFORE COMPLETING FORM
1. REPORT NUMBER AFIT/CI/NR 87-67T	2. GOVT ACCESSION NO.	3. RECIPIENT'S CATALOG NUMBER
4. TITLE (and Subtitle) Radiant Power Degradation Of Silicon-Doped Gallium Arsenide And Gallium Aluminum Arsenide Infrared Light-Emitting Diodes	5. TYPE OF REPORT & PERIOD COVERED THESIS/DISSERTATION	
	6. PERFORMING ORG. REPORT NUMBER	
7. AUTHOR(s) William Nodin Resimont	8. CONTRACT OR GRANT NUMBER(s)	
9. PERFORMING ORGANIZATION NAME AND ADDRESS AFIT STUDENT AT: University of Arkansas	10. PROGRAM ELEMENT, PROJECT, TASK AREA & WORK UNIT NUMBERS	
11. CONTROLLING OFFICE NAME AND ADDRESS AFIT/NR WPAFB OH 45433-6583	12. REPORT DATE May 1987	
	13. NUMBER OF PAGES 66	
14. MONITORING AGENCY NAME & ADDRESS (if different from Controlling Office)	15. SECURITY CLASS. (of this report)  UNCLASSIFIED	
	15a. DECLASSIFICATION/DOWNGRADING SCHEDULE	
16. DISTRIBUTION STATEMENT (of this Report)  APPROVED FOR PUBLIC RELEASE; DISTRIBUTION UNLIMITED		
17. DISTRIBUTION STATEMENT (of the abstract entered in Block 20, if different from Report)		
18. SUPPLEMENTARY NOTES APPROVED FOR PUBLIC RELEASE: IAW AFR 190-1		<i>Lynn E. Wolaver</i> LYNN E. WOLAVER 17 May 87 Dean for Research and Professional Development AFIT/NR
19. KEY WORDS (Continue on reverse side if necessary and identify by block number)		
20. ABSTRACT (Continue on reverse side if necessary and identify by block number) ATTACHED		

RADIANT POWER DEGRADATION  
OF  
SILICON-DOPED  
GALLIUM ARSENIDE  
AND  
GALLIUM ALUMINUM ARSENIDE  
INFRARED LIGHT-EMITTING DIODES



Accession For	
NTIS GRA&I	<input checked="" type="checkbox"/>
DTIC TAB	<input type="checkbox"/>
Unannounced	<input type="checkbox"/>
Justification	
By	
Distribution/	
Availability Codes	
Dist.	Avail and/or Special
A-1	

ABSTRACT


The I-V characteristics support the theory that radiant power degradation in GaAs:Si and GaAlAs:Si IREDS is linked to a decrease in the internal quantum efficiency.


This thesis is approved for  
recommendation to the  
Graduate Council

Thesis Adviser:

  
\_\_\_\_\_  
J. R. Yeargan

Thesis Committee:

  
\_\_\_\_\_  
W. D. Brown

  
\_\_\_\_\_  
R. L. Brown

  
\_\_\_\_\_  
H. A. Naseem

THESIS DUPLICATION RELEASE

I hereby authorize the University of Arkansas Libraries to duplicate this thesis when needed for research and/or scholarship.

Agreed William N. Resumont

Refused \_\_\_\_\_



## ACKNOWLEDGEMENTS

I thank God and my Lord, Jesus Christ, for giving me the strength to continue this endeavor.

I would like to offer my sincere appreciation to Dr. J.R. Yeargan for his support during this project. His guidance in the beginning of the work provided a clear path to follow, and his advice throughout the research helped minimize the difficulties. His expertise was especially helpful in interpreting the results. I also wish to express my gratitude to BEI Electronics and AGL Corporation for providing the funding and the necessary equipment. In addition, I thank the United States Air Force for allowing me to study at the University of Arkansas.

My deepest thanks goes out to my wife, Barbara, for the love she showed during the completion of this thesis. Her devotion provided the stability in my home life that made the completion possible. Also, I would like to thank my children, Skipper, Shaun, Jay, Matthew, and Emily, for encouraging me in my times of trials. I want to take this opportunity to encourage them to obtain the highest level of education possible.

This thesis is dedicated to my loving parents, Bill and Zeta Resimont, my grandparents, W.J. and Toni Nordin, and my late grandparents, W.L and Ina Resimont.

TABLE OF CONTENTS

	Page
LIST OF FIGURES.....	vi
LIST OF TABLES.....	viii
ABSTRACT.....	ix
I. INTRODUCTION.....	1
II. DIODE CHARACTERISTICS.....	3
III. MEASUREMENT SYSTEM.....	17
IV. MEASUREMENT RESULTS.....	25
V. SUMMARY.....	54
REFERENCES.....	55
APPENDIX I.....	56
APPENDIX II.....	57
APPENDIX III.....	60
APPENDIX IV.....	62
APPENDIX V.....	65

LIST OF FIGURES

Figure	Page
1. C-V Characteristics Measuring System.....	18
2. I-V Characteristics Measuring System.....	20
3. P-I-V Characteristics Measuring System.....	22
4. Stressing Circuits.....	23
5. Normalized Radiant Power vs Time (G1-G4).....	25
6. Normalized Radiant Power vs Time (G5-G8).....	26
7. Normalized Radiant Power vs Time (J1,J3-J5).....	27
8. Normalized Radiant Power vs Time (J6-J8,J0).....	28
9. Normalized Radiant Power vs Time (H1-H4).....	29
10. Normalized Radiant Power vs Time (H5-H8).....	30
11. Normalized Radiant Power vs Time (X1-X4).....	31
12. Normalized Radiant Power vs Time (X5-X8).....	32
13. Normalized Radiant Power vs Time (J2,J9).....	33
14. C-V Characteristics (J2).....	34
15. Normalized C-V Characteristics (J2).....	35
16. Normalized C-V Characteristics (X5).....	36
17. Doping Profile (J2).....	37
18. Normalized Doping Profile (J2).....	38
19. Normalized Doping Profile (X5).....	39
20. Reverse I-V Characteristics (J2).....	40
21. Normalized Reverse I-V Characteristics (J2).....	41
22. Normalized Reverse I-V Characteristics (X5).....	42
23. Forward I-V Characteristics (J2).....	43
24. Normalized Forward I-V Characteristics (J2).....	44

25.	Normalized Forward I-V Characteristics (X5).....	45
26.	Internal Quantum Efficiency vs Time (X5-X8).....	46
27.	Reverse I-V Characteristics (X4).....	47
28.	Normalized Reverse I-V Characteristics (X4).....	48
29.	Reverse I-V Characteristics w/Temp (X4).....	49
30.	Forward I-V Characteristics (X4).....	50
31.	Forward Log I-V Characteristics (X4).....	51
32.	Forward Log I-V Characteristics w/Temp (X4).....	52
33.	Forward Log I - Log V Characteristics (X4).....	53

must traverse before they reach the junction. At low currents, the voltage drop across this resistance is insignificant, but at higher currents, the voltage drop becomes quite large, and thus, the diffusion current is limited. Second, the limiting forward bias across a p-n junction is equal to the contact potential. When the forward bias approaches the contact potential, the minority carrier injection level is comparable to the majority carrier concentration. This results in the breakdown of the diode equation.[2, Page 178] Due to the complexity that series resistance and high level injection introduces to (19), this work will neglect them.

#### D. Radiant Power-Current-Voltage

Radiant power (P) is defined as

$$P = Q_e E_p I_F \quad (23)$$

where

$Q_e$  = the external quantum efficiency

$E_p$  = the effective photon energy (eV)

$I_F$  = the forward current (amperes)

The external quantum efficiency is an indication of how well a light-emitting diode converts electrical energy into light. Its units are photons per electron, but in reality, it requires many electrons to produce one photon.

Therefore,  $Q_e$  is always less than unity. A relationship describing  $Q_e$  is

$$Q_e = Q_i M_i \quad (24)$$

where

$Q_i$  = the internal quantum efficiency

$M_i$  = the minority-carrier injection efficiency

The internal quantum efficiency is defined as

$$Q_i = R_r / (R_r + R_{nr}) \quad (25)$$

where

$R_r$  = the radiative recombination rate

$R_{nr}$  = the non-radiative recombination rate

In order for radiative recombination to take place, the semiconductor material should possess a direct energy gap.[5, Page 27] Both GaAs:Si and GaAlAs:Si have direct energy gaps. However, GaAlAs:Si changes to an indirect energy gap semiconductor if Al is over about 40% of the total Ga and Al concentration.[12, Page 295] The major radiative transition for these IREDS is between the conduction band and the Si acceptor level.[4, Page 148] For GaAs:Si, this results in an effective photon energy ( $E_p$ ) of about 1.33 eV, or a photon wavelength of 935 nanometers. For GaAlAs:Si, the photon wavelength is about 880 nanometers corresponding to  $E_p = 1.41$  eV.

Another mechanism by which radiative recombinations occur is known as exciton transitions.[4, Page 146] An exciton state can be visualized as an electron and hole that orbit around their common center of gravity at large distances. They are found in relatively pure semiconductor materials at low temperatures.

Non-radiative recombination mechanisms include the Auger effect, surface recombinations, and multiple phonon emissions.[3, Chapter 7] The Auger effect is a three-body collision where the energy from an electron-hole recombination is immediately absorbed by another electron or hole deep in the conduction or valence bands. The energy is then released as heat to the lattice. It is important to note that the Auger effect can occur via any energy level transition and should become more intense as the carrier concentration increases. Surface recombination takes place at dangling bonds that can absorb impurities from the ambient. They are modeled as continuous distributions of surface states. A localized defect is also modeled as a continuum of states and can be considered an internal surface. Multiple-phonon emission happens when non-radiative recombination takes place other than through a continuum of states. Since the expected loss of energy during recombination is much greater than the energy of one phonon, a cascade of phonons must be released.

The minority carrier injection efficiency is

$$M_i = I_{Fd}/I_F \quad (26)$$

Substitution of (26) in (24) gives

$$Q_e = Q_i I_{Fd}/I_F \quad (27)$$

Substitution of (27) in (23) gives

$$P = Q_i E_p I_{Fd} \quad (28)$$

Substitution of (14) and (15) in (28) gives

$$P = Q_i E_p I_{do} [\exp(V/nV_t) - 1] \quad (29)$$

Let

$$P_o = Q_i E_p I_{do} \quad (30)$$

Substitution of (30) in (29) gives

$$P = P_o [\exp(V/nV_t) - 1] \quad (31)$$

Assuming  $V \gg V_t$ , taking the logarithm of both sides of (31) gives

$$\log P = \log P_o - \frac{\log e}{nV_t} V \quad (32)$$



A plot of  $\log P$  vs  $V$  should yield a straight line with the following parameters:

$$\text{slope} = \frac{\log e}{nV_t} \quad (33)$$

$$\text{y-intercept} = \log P_0 \quad (34)$$

Rearranging (27) gives

$$Q_i/Q_e = I_F/I_{Fd} \quad (35)$$

Assuming  $V \gg V_t$ , substitution of (14), (15), and (19) in (35) gives

$$Q_i/Q_e = 1 + (I_{r0}/I_{d0})\exp[(-V/nV_t)(1 - n/m)] \quad (36)$$

Let

$$g = 1 - n/m \quad (37)$$

Substitution of (37) in (36) gives

$$Q_i/Q_e = 1 + (I_{r0}/I_{d0})[\exp(-V/nV_t)]^g \quad (38)$$

With  $V \gg V_t$ , rearranging (31) gives

$$P_0/P = \exp(-V/nV_t) \quad (39)$$

Substitution of (39) in (38) gives

$$Q_i/Q_e = 1 + (I_{r0}/I_{d0})(P_0/P)^g \quad (40)$$

or

$$\frac{1}{Q_e} = \frac{1}{Q_i} [1 + (I_{ro}/I_{do})(P_o/P)^g] \quad (41)$$

A plot of  $1/Q_e$  vs  $1/P^g$  should yield a straight line with the following parameters:

$$\text{slope} = (I_{ro}/I_{do})(P_o^g/Q_i) \quad (42)$$

$$\text{y-intercept} = 1/Q_i \quad (43)$$

Care must be taken in determining (42) and (43) due to the problems associated with series resistance and high injection levels. These problems can be eliminated by measuring radiant power at low current levels.

CHAPTER III  
MEASUREMENT SYSTEM

A. Capacitance-Voltage Characteristics

The capacitance-voltage (C-V) characteristics are measured using a Hewlett-Packard Model 4280A (HP4280A) 1 MHz C Meter/C-V Plotter. Basic measurement accuracy is 0.1%, and measurement resolution is 1E-15 farads.[7] The diode to be tested is placed in a Hewlett-Packard Model 16058A (HP16058A) Test Fixture [8] with an HP16058-60008 Socket Board specifically designed for diodes. The HP4280A and the HP16058A are connected with 1 meter coaxial cables equipped with HP34116A BNC-TRIAX adapters. To keep the temperature constant at 35°C, the HP16058A is placed in a Delta Design Model 2300 (DD2300) Environmental Test Chamber equipped with a TYPE V Controller (Microcomputer Based). Basic deviation from temperature set point is 0.05°C.[9] The entire system is controlled via General Purpose Interface Bus (GPIB) connections with a Texas Instruments Personal Computer (TI-PC). A BASIC program allows the HP4280A to extract the stray capacitance from the measurements due to the cables and test fixture. The parasitic capacitance of the diode package is neglected. LOTUS 1-2-3 Graphics software is employed to plot graphs on a Texas Instruments OMNI 800/Model 855 printer. Figure 1 shows a block diagram of the C-V characteristics measuring system.

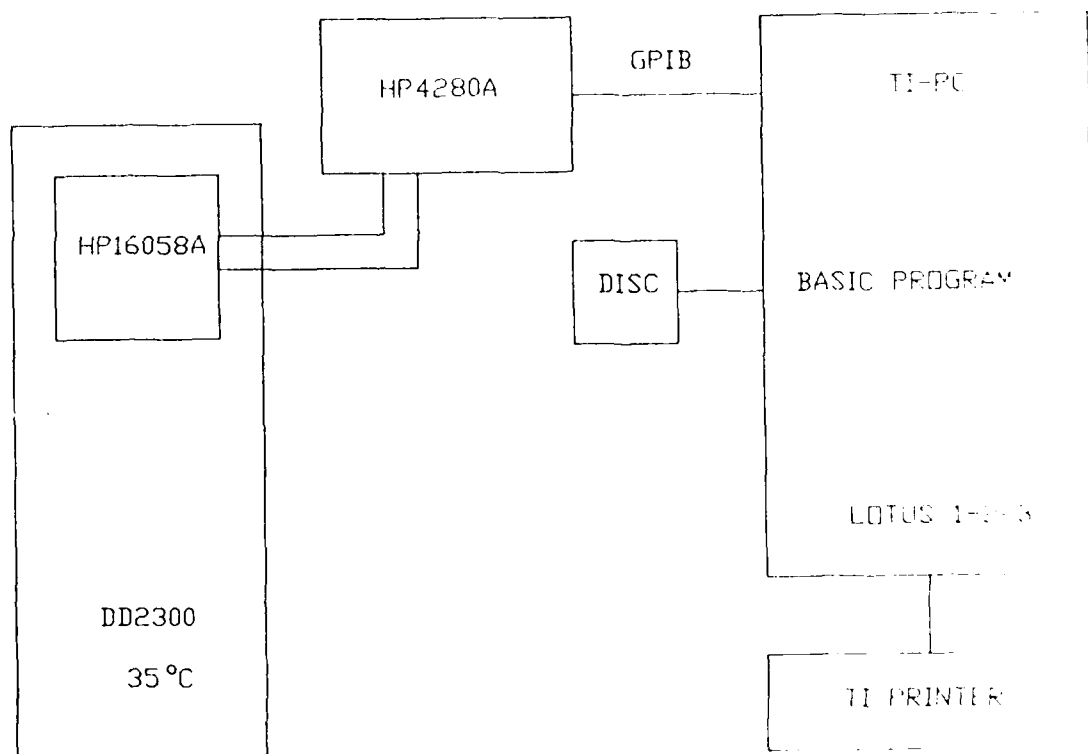


Figure 1. C-V Characteristics Measuring System

## B. Current-Voltage Characteristics

The current-voltage (I-V) characteristics are measured using a Hewlett-Packard Model 4145A (HP4145A) Semiconductor Parameter Analyzer. Basic measurement accuracy is 0.5%, and measurement resolution is  $1\text{E-}12$  amperes and  $1\text{E-}13$  volts.[10] The diode to be tested is placed in a Hewlett-Packard Model 16058A (HP16058A) Test Fixture [8] with an HP16058-60008 Socket Board specifically designed for diodes. The HP16058A provides shielding to reduce the effects of stray current noise. It allows accurate measurements in the  $1\text{E-}12$  ampere range. The HP4145A and the HP16058A are connected with 3 meter triaxial cables. To keep the temperature constant at  $35^{\circ}\text{C}$ , the HP16058A is placed in a Delta Design Model 2300 (DD2300) Environmental Test Chamber equipped with a Type V Controller (Microcomputer Based). Basic deviation from temperature set point is  $0.05^{\circ}\text{C}$ . The entire system is controlled via General Purpose Interface Bus (GPIB) connections with a Texas Instruments Personal Computer (TI-PC). The data is stored on a floppy disc using a BASIC program. Front panel controls on the HP4145A create graphs on a Hewlett-Packard Model 7550A Graphics Plotter. Additional graphs are made using LOTUS 1-2-3 Graphics software and a Texas Instruments OMNI 800/Model 855 printer. Figure 2 shows a block diagram of the I-V characteristics measuring system.

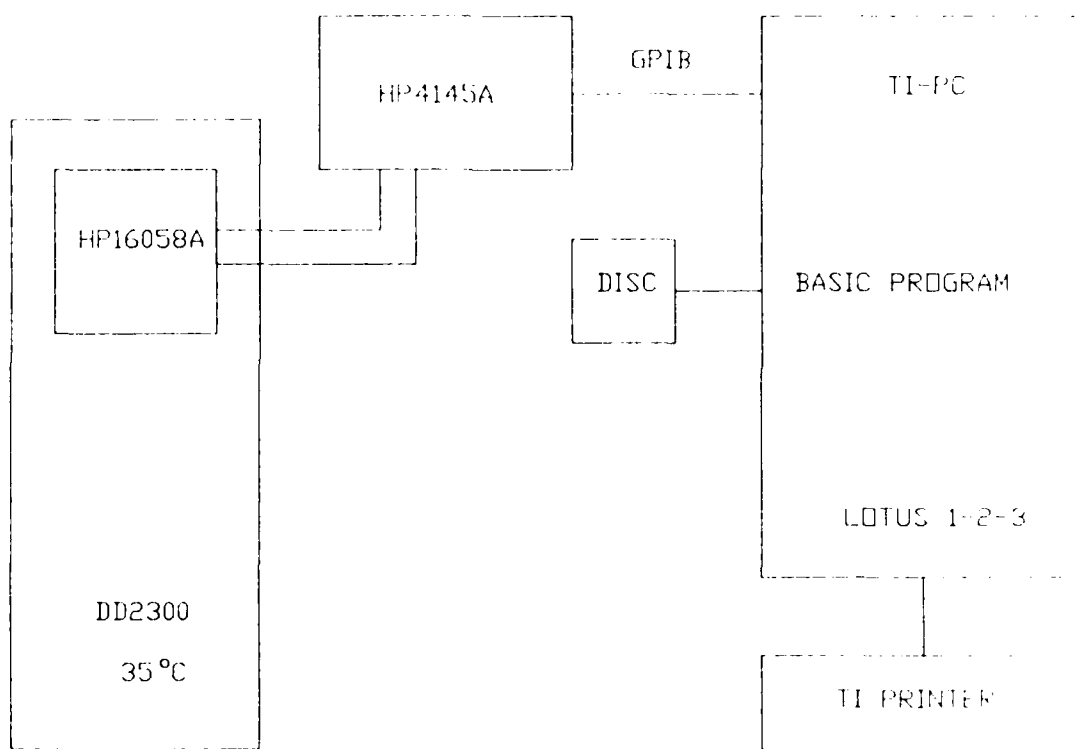


Figure 2. I-V Characteristics Measuring System

### C. Radiant Power-Current-Voltage Characteristics

The radiant power-current-voltage characteristics (P-I-V) are measured using a United Detector Technology Model 61AC (UDT61AC) Optometer, a United Detector Technology Model 2575R (UDT2575R) Integrating Sphere with a silicon detector, and a Hewlett-Packard Model 4145A (HP4145A) Semiconductor Parameter Analyzer. Basic measurement accuracy for the UDT61AC is 1.2%, and measurement resolution is  $1\text{E}-8$  watts.[11] Basic measurement accuracy for the UDT2575R is 7% over a wavelength range of 450 to 950 nanometers. Basic measurement accuracy for the HP4145A is 0.5%, and measurement resolution is  $1\text{E}-12$  amperes and  $1\text{E}-3$  volts.[10] The diode to be tested is placed in a fixture inside a Delta Design Model 2300 (DD2300) Environmental Test Chamber equipped with a Type V Controller (Microcomputer Based). The temperature is set at  $35^{\circ}\text{C}$  with basic deviation of  $0.05^{\circ}\text{C}$ .[9] The P-I-V characteristics are manually recorded and entered into a Texas Instruments Personal Computer (TI-PC). The data is stored on a floppy disc using a BASIC program. LOTUS 1-2-3 Graphics software is employed to obtain graphs on a Texas Instruments OMNI 800/Model 855 printer. The procedure for measuring radiant power is included in APPENDIX III. Figure 3 shows a block diagram of the P-I-V characteristics measuring system.

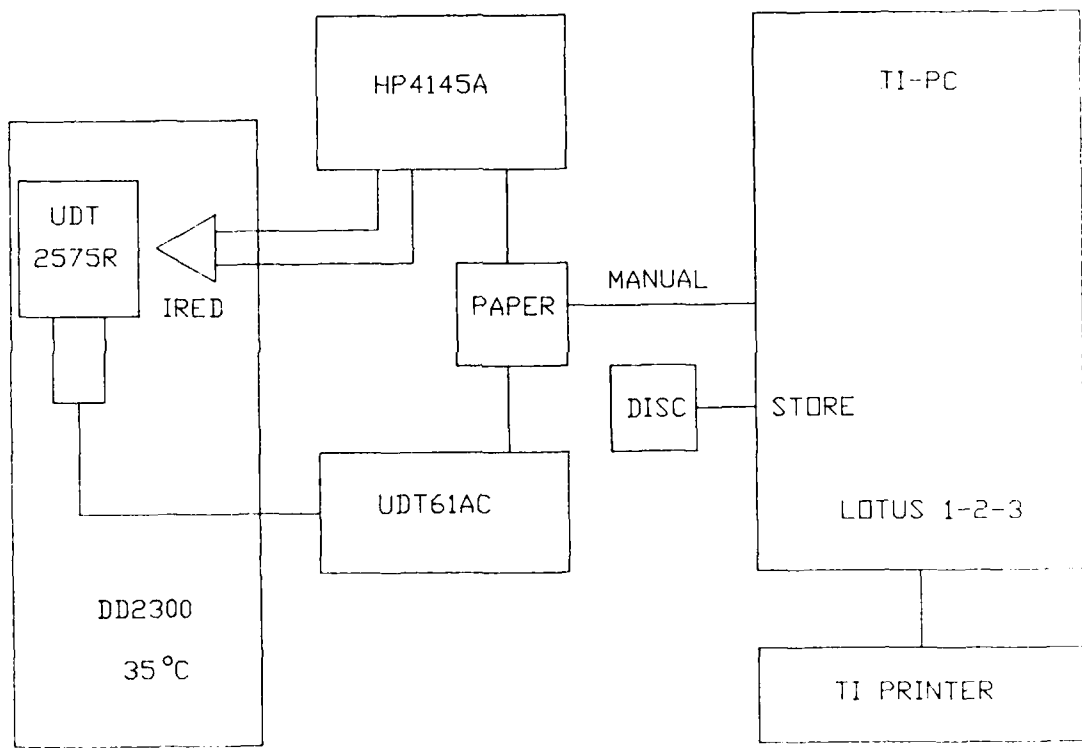


Figure 3. P-I-V Characteristics Measuring System



#### D. Stressing Circuits and Diodes

The power source for the stressing circuits is a Hewlett-Packard Model 6205B (HP6205B) Dual DC Power Supply. The HP6205B is equipped with 2 analog meters that allow the current levels to be monitored. Two separate Archer Universal Breadboards contain the stressing circuits. One circuit is stressed at 100 mA DC and consists of 16 infrared-emitting diodes mounted in series: 4 Honeywell SE5450 [14, Page 46], 4 Honeywell SE3470 [14, Page 48], 4 TRW OP131 [15, Page 6], and 4 TRW OP233. [15, Page 22] The second circuit is stressed at 200 mA DC and is composed of 16 identical infrared-emitting diodes. An aluminum heat sink with a case-to-ambient thermal resistance of approximately  $34^{\circ}\text{C}/\text{W}$  is provided for each diode. The calculations supporting this heat sink value are included in APPENDIX IV. Figure 4 shows a block diagram of the stressing circuits. Table 2 provides information about the current densities and junction temperatures of each IRED under stress conditions. The calculations supporting the junction temperature values are included in APPENDIX V. Control diodes J2 and J9 were not stressed.

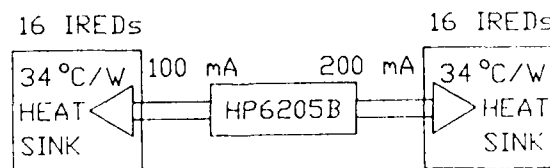


Figure 4. Stressing Circuits

LAB. NAME	COMPANY NAME	STRESS CURRENT (A)	JUNCTION AREA (cm <sup>2</sup> )	CURRENT DENSITY (A/cm <sup>2</sup> )	JUNCTION TEMP. (°C)	MATERIAL
G1-G4	HW SE5450	.100	7.74E-4	129	52	GaAs <sub>1</sub> Si
G5-G8	HW SE5450	.200	7.74E-4	258	83	GaAs <sub>1</sub> Si
H1-H4	HW SE3470	.100	2.09E-3	48	54	GaAlAs <sub>1</sub> Si
H5-H8	HW SE3470	.200	2.09E-3	96	86	GaAlAs <sub>1</sub> Si
J1 J3-J5	TRW DP131	.100	6.45E-4	155	55	GaAs <sub>1</sub> Si
J6-J8 J0	TRW DP131	.200	6.45E-4	310	89	GaAs <sub>1</sub> Si
X1-X4	TRW DP233	.100	6.45E-4	155	55	GaAlAs <sub>1</sub> Si
X5-X8	TRW DP233	.200	6.45E-4	310	90	GaAlAs <sub>1</sub> Si

Table 2. IRED Stressing Conditions

CHAPTER IV  
MEASUREMENT RESULTS

Figure 5 shows the normalized radiant power as a function of time for 4 Honeywell SE5450 GaAs:Si IREDS. The radiant power is normalized to the initial conditions in order to show the changes in radiant power with time. The stressing conditions included a current density of 129 A/cm<sup>2</sup> and a junction temperature of 52°C. Notice that the average degradation after 1000 hours of stress shows a ratio of about 0.98. This is equivalent to a 2% decrease in radiant power.

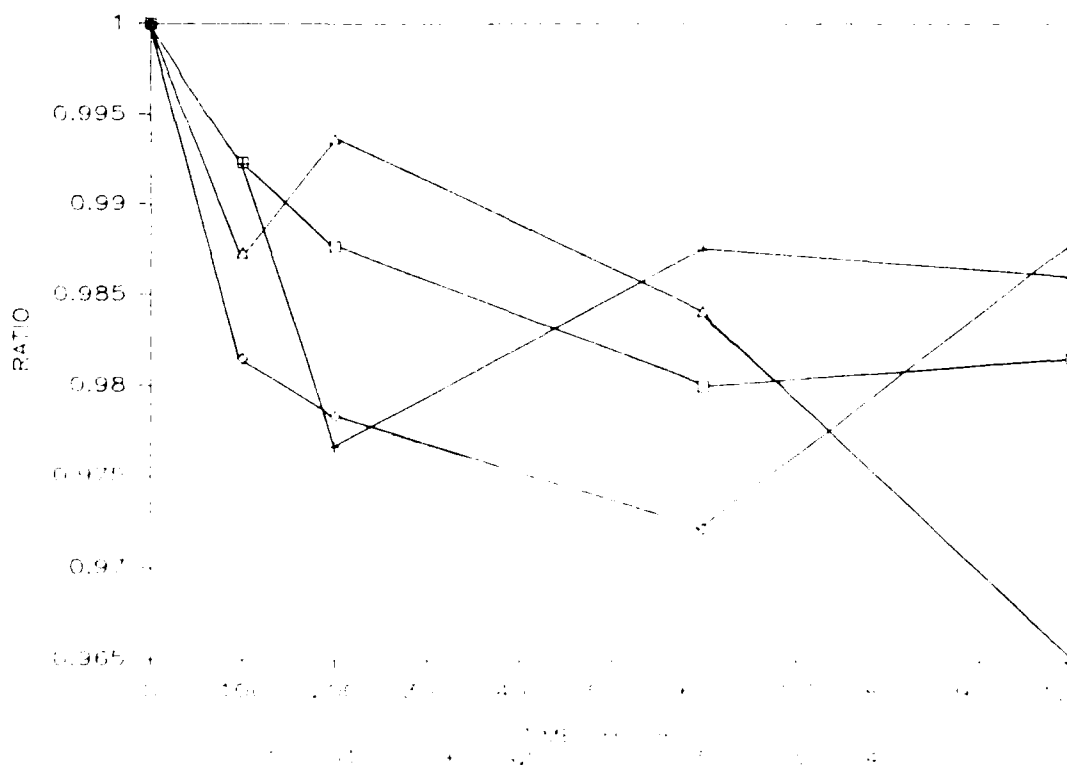


Figure 5. Normalized Radiant Power vs. Time (31-34)

Figure 6 shows the normalized radiant power as a function of time for 4 of the same type of IREDs shown in Figure 5, but the stressing conditions were approximately doubled with a current density of 258 A/cm<sup>2</sup> and a junction temperature of 83°C. Notice that the average degradation after 1000 hours of stress shows a ratio of about 0.96 or a 4% decrease in radiant power. This is approximately double the degradation exhibited by the IREDs in Figure 5. Also, both Figures 5 and 6 display a scattering of data points that is typical of radiant power measurements. An averaging of several data points should eliminate this effect.

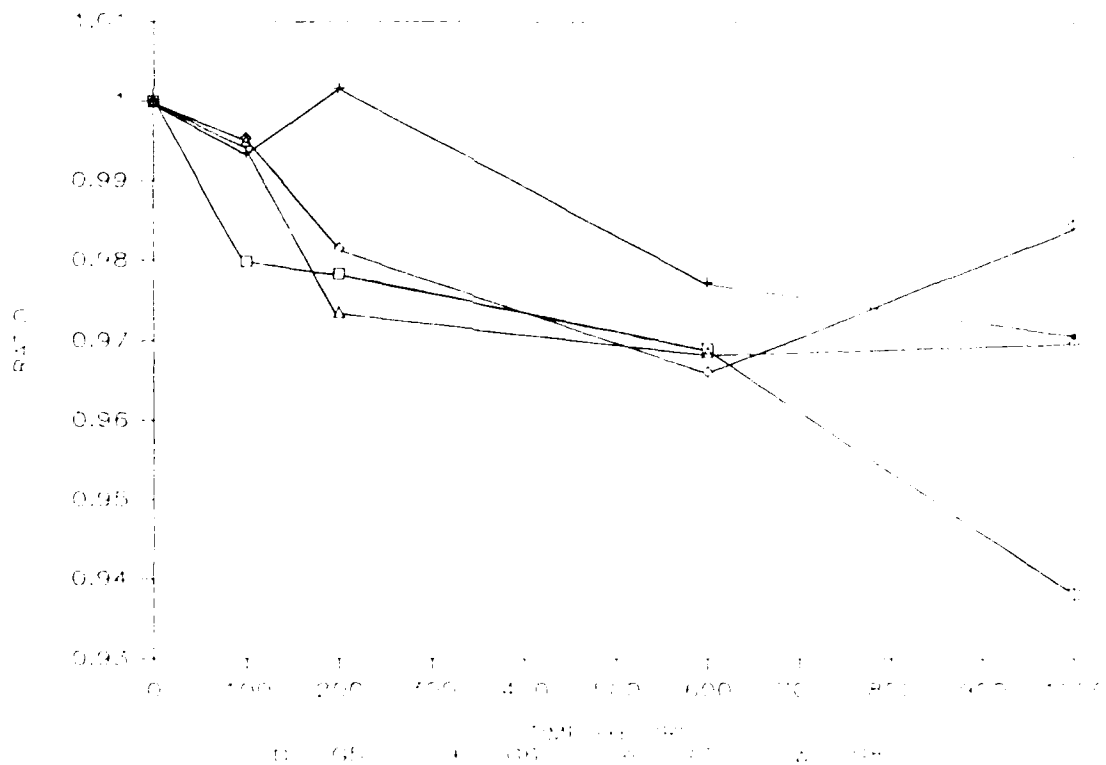


Figure 6. Normalized Radiant Power vs Time (G5-G8)

Figure 7 shows the normalized radiant power as a function of time for 4 TRW OP131 GaAs:Si IREDS. The stressing conditions included a current density of  $155 \text{ A/cm}^2$  and a junction temperature of  $55^\circ\text{C}$ . Notice that the average degradation after 1000 hours of stress shows a ratio of about 0.85 or a decrease of 15% in radiant power. This is significantly higher than the IREDS in Figure 5 although the stressing conditions were approximately the same. However, the wide variation in the degradation rates indicates that this may not be a representative sample of the IREDS as a whole.

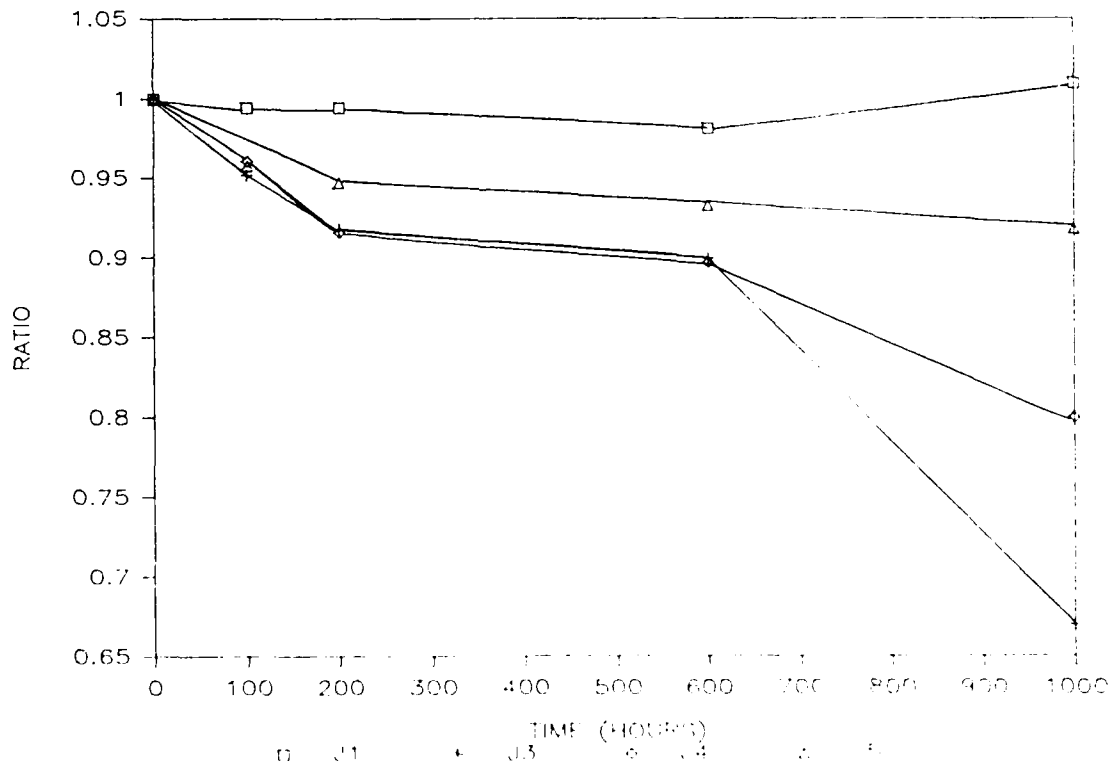


Figure 7. Normalized Radiant Power vs Time (J1, J3-J5)

Figure 8 shows the normalized radiant power as a function of time for 4 of the same type of IREDs shown in Figure 7, but the stressing conditions were approximately doubled with a current density of  $310 \text{ A/cm}^2$  and a junction temperature of  $89^\circ\text{C}$ . Notice that the average degradation after 1000 hours of stress shows a ratio of about 0.6 or a decrease of 40% in radiant power. Although the stressing conditions were only about 15% higher than those for the IREDs in Figure 6, the degradation is about 10 times greater. Also, the degradation rate closely resembles a decreasing exponential.

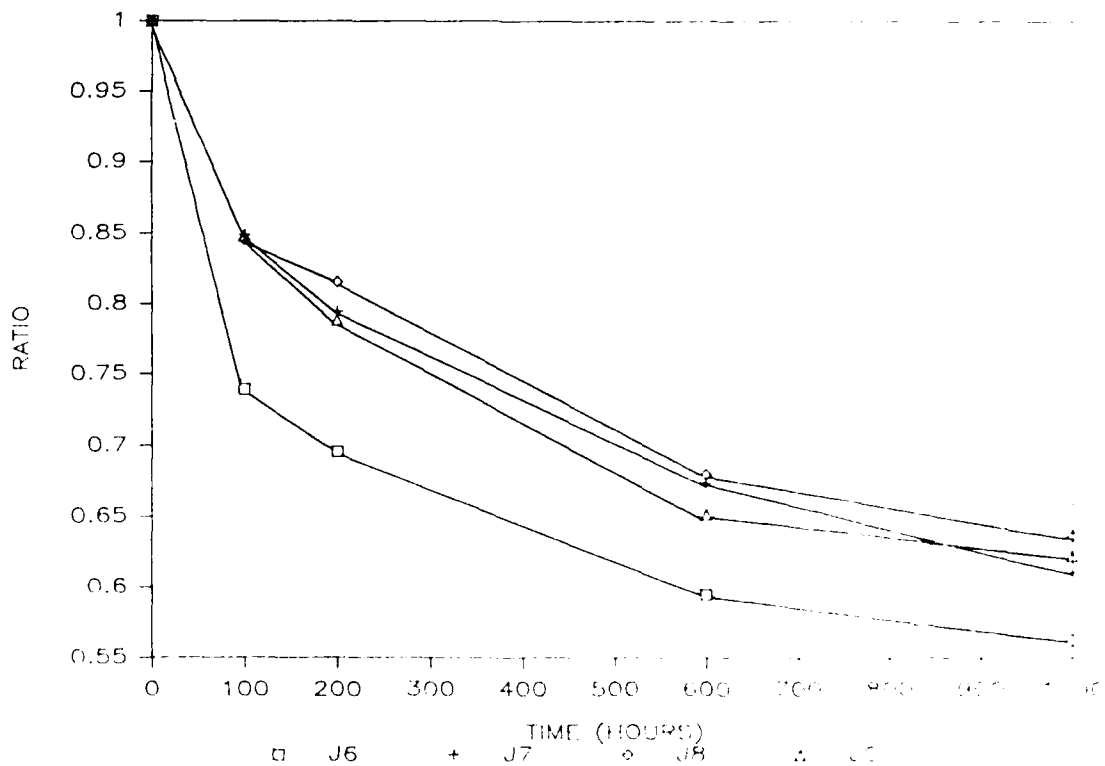


Figure 8. Normalized Radiant Power vs Time (J6-J8, J0)

Figure 9 shows the normalized radiant power as a function of time for 4 Honeywell SE3470 GaAlAs:Si IREDS. The stressing conditions included a current density of 48 A/cm<sup>2</sup> and a junction temperature of 54°C. Notice that two distinct degradation rates are evident with the major difference being the degradation during the first 100 hours of stress. Both degradation rates appear to level off after 100 hours of stress. These degradation rates compare with those shown by the IREDS in Figure 7. However, the stressing conditions of the IREDS in Figure 7 were about 70% higher.

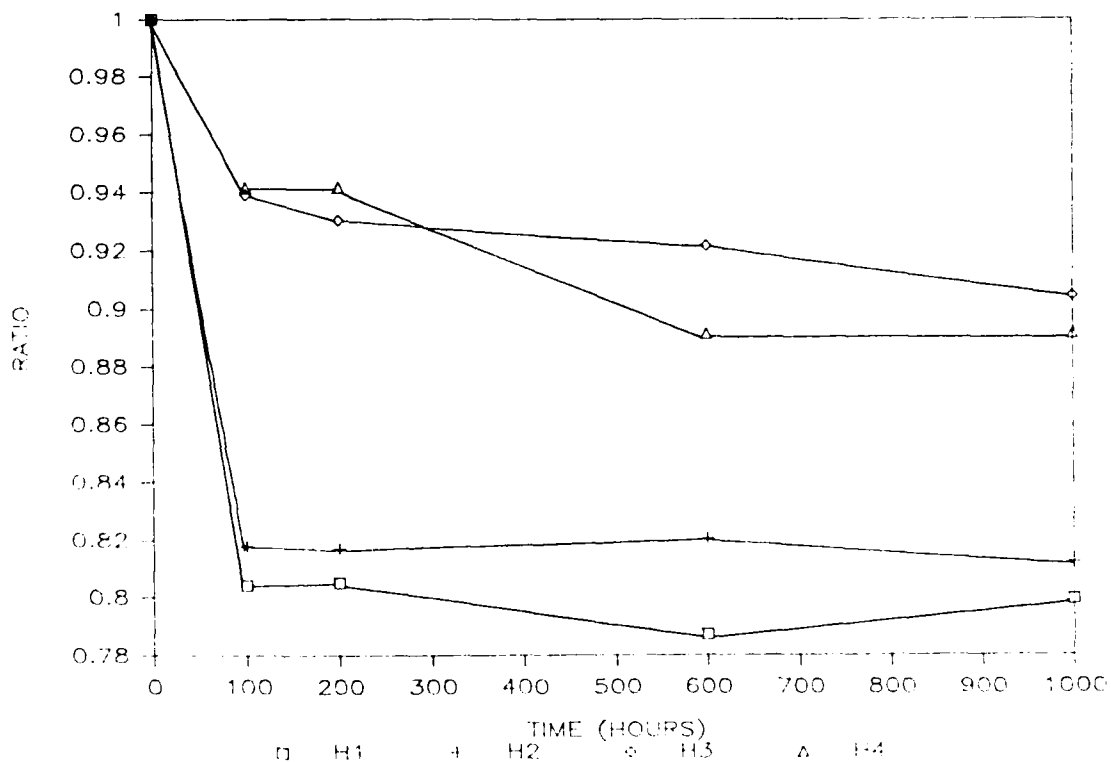


Figure 9. Normalized Radiant Power vs Time (H1-H4)

Figure 10 shows the normalized radiant power as a function of time for 4 of the same type of IREDS shown in Figure 9, but the stressing conditions were approximately doubled with a current density of  $96 \text{ A/cm}^2$  and a junction temperature of  $86^\circ\text{C}$ . Notice that the average degradation after 1000 hours of stress shows a ratio of about 0.78 or a decrease of 22% in radiant power. Although this degradation is not significantly higher than that shown by the IREDS in Figure 9, the shape of the curves in Figure 10 indicates that the degradation is approaching failure at a faster rate.

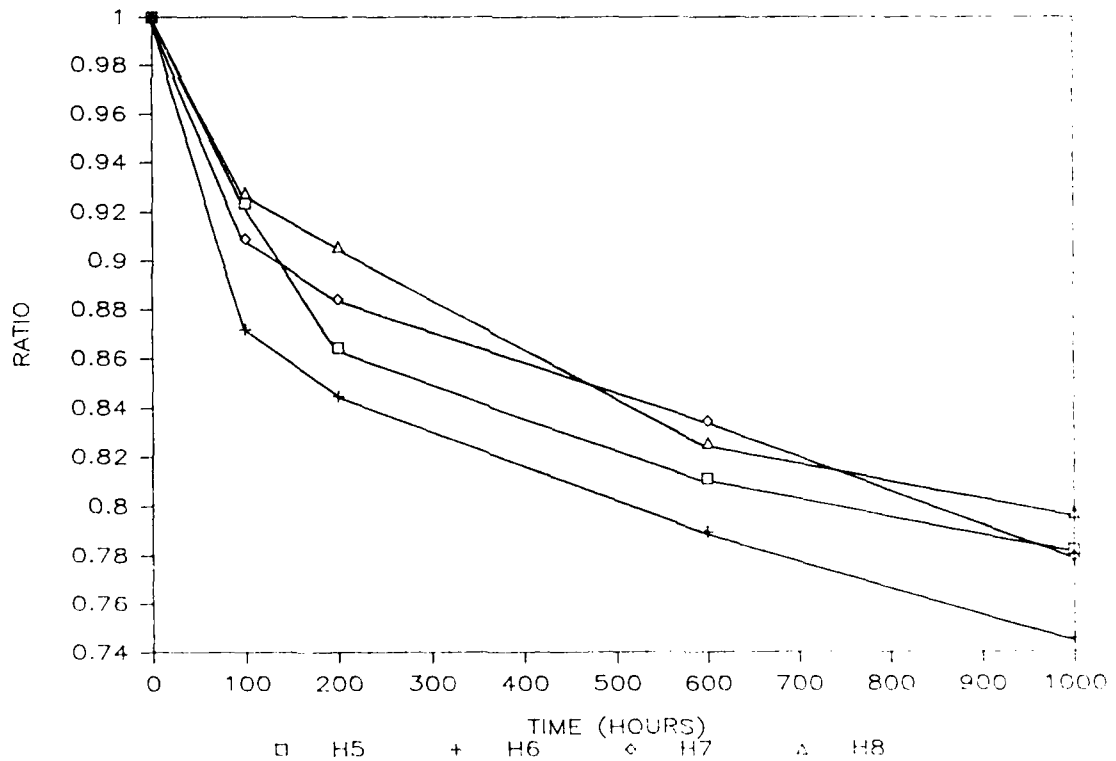


Figure 10. Normalized Radiant Power vs Time (H5-H8)



Figure 11 shows the normalized radiant power as a function of time for 4 TRW OP233 GaAlAs:Si IREDS. The stressing conditions included a current density of 155 A/cm<sup>2</sup> and a junction temperature of 55°C. Notice that the average degradation after 1000 hours of stress shows a ratio of about 0.9 or a decrease of 10% in radiant power. This degradation is approximately the same as that shown by the IREDS in Figure 9, but the degradation rate of the IREDS in Figure 11 is more gradual. In addition, the stressing conditions of the IREDS in Figure 9 were about 70% lower.

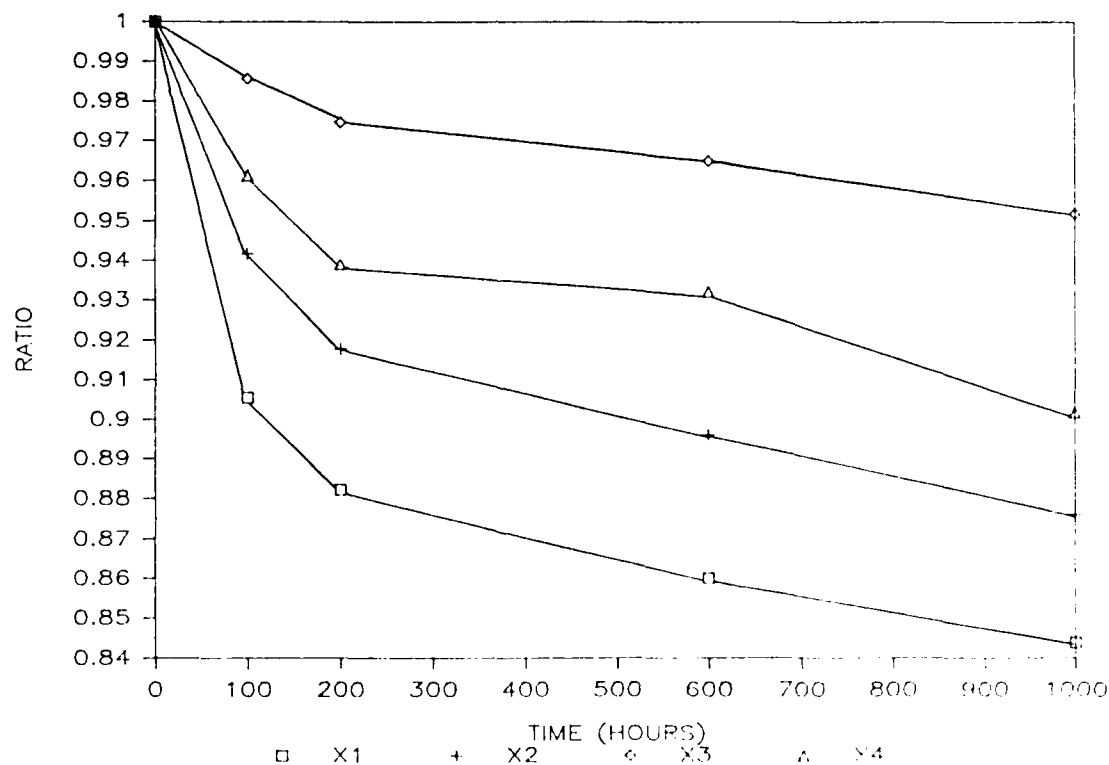


Figure 11. Normalized Radiant Power vs Time (X1-X4)

Figure 12 shows the normalized radiant power as a function of time for 4 of the same type of IREDS shown in Figure 11, but the stressing conditions were approximately doubled with a current density of  $310 \text{ A/cm}^2$  and a junction temperature of  $90^\circ\text{C}$ . Notice that IRED X6 displays a slower degradation rate than the other IREDS. The remaining IREDS show degradation rates similar to those displayed by the IREDS in Figure 8. The stressing conditions of the IREDS in Figures 8 and 12 were virtually identical. In addition, Figures 8 and 12 display the degradation rates of GaAs:Si and GaAlAs:Si IREDS, respectively.

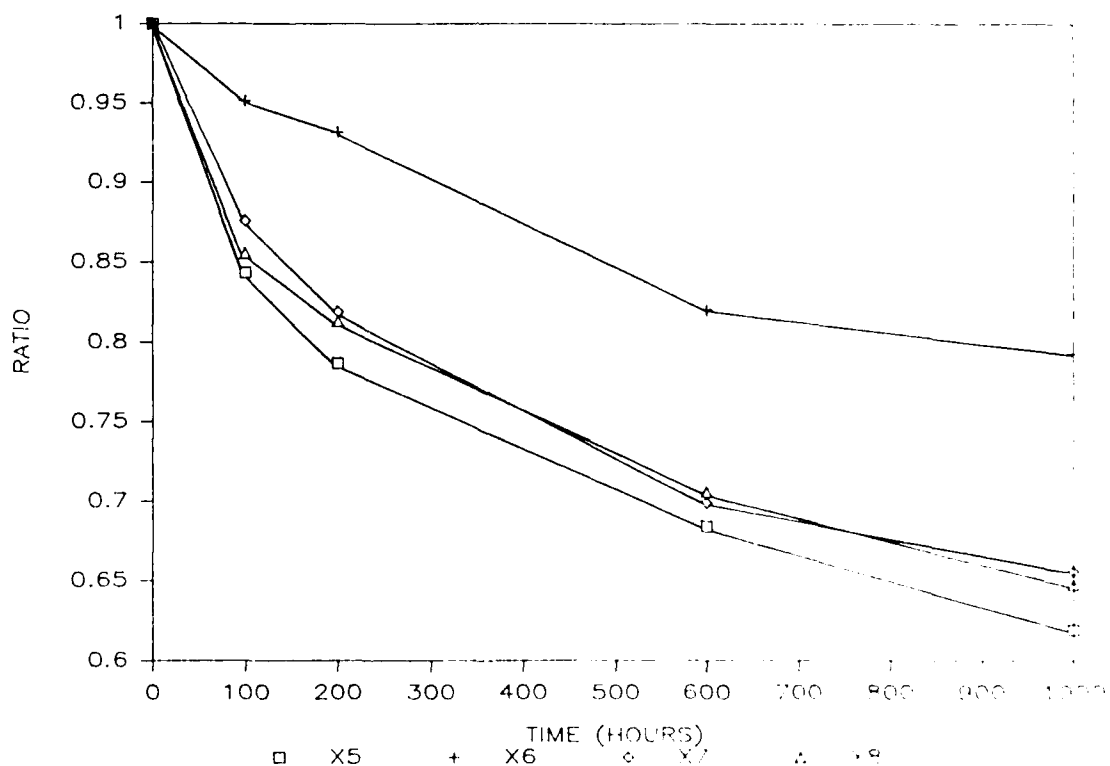


Figure 12. Normalized Radiant Power vs Time (X5-X8)

Figure 13 shows the normalized radiant power vs time for 2 TRW OP131 GaAs:Si IREDS. These control IREDS were not stressed and thus were assumed not to degrade. This assumption appears valid since Figure 13 shows that the radiant power did not vary more than 1% from the initial conditions. Although GaAlAs:Si control IREDS were not included in this work, it was assumed that comparisons between stressed GaAlAs:Si IREDS and control GaAs:Si IREDS remain valid. However, further research should include a control IRED for each type of IRED studied as well as for each different manufacturer.

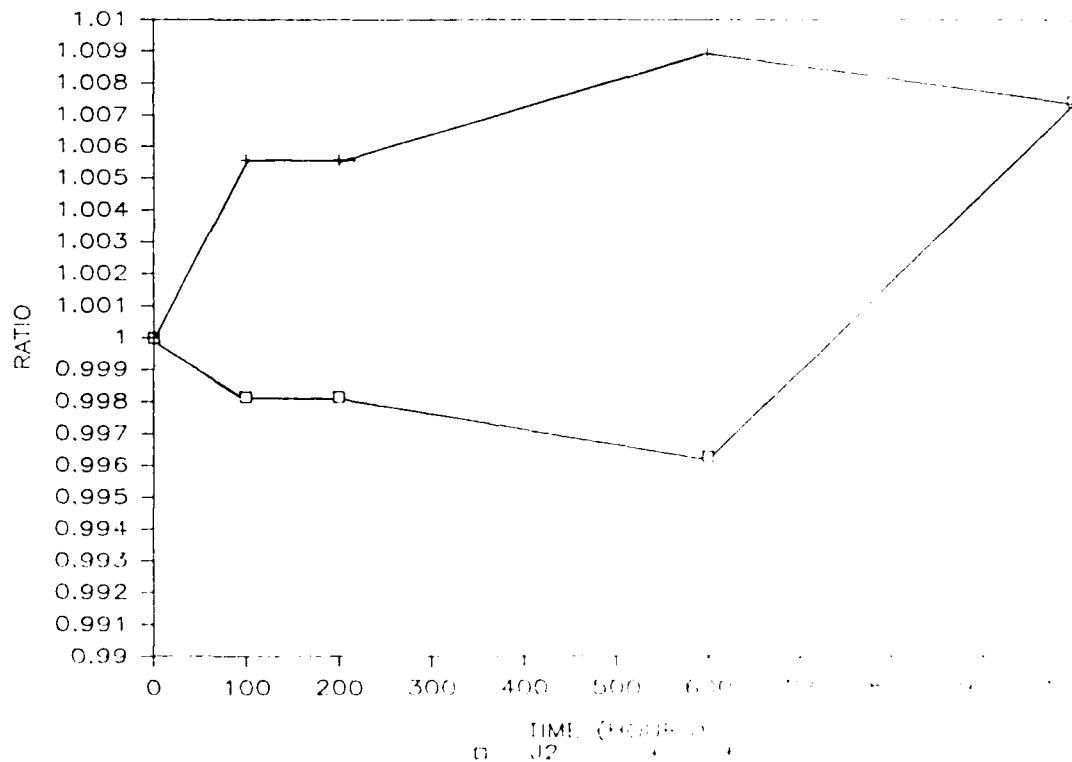


Figure 13. Normalized Radiant Power vs Time (11, 199)

Figures 5 through 12 emphasize the varying rates of radiant power degradation that IREDS exhibit. Although the degradation is a result of the stressing conditions, the same stressing conditions may have diverse affects on IREDS made from different materials by different manufacturers. The object of this work is to use the C-V, I-V, and P-I-V characteristics to identify IRED failures regardless of their physical make-up or manufacturer. The remainder of this chapter will compare the characteristics of control IRED J2 with IREDS X4 and X5 to show the affects of stress. Figure 14 shows the C-V characteristics of J2.

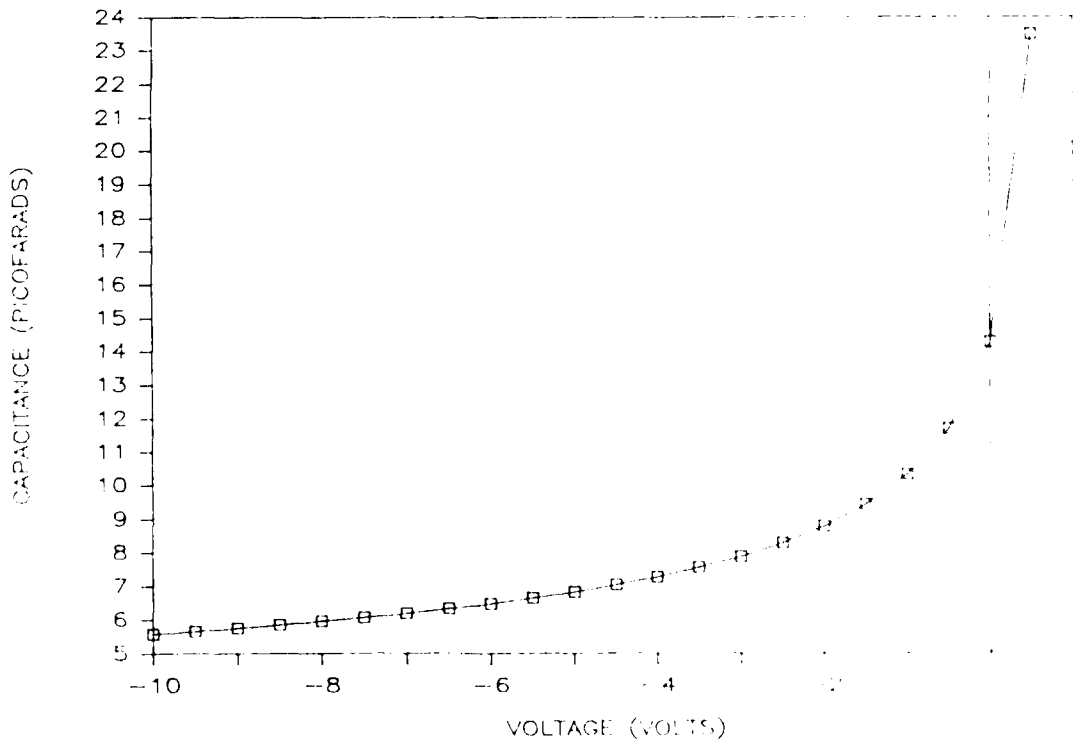


Figure 14. C-V Characteristics (J2)

Figure 15 shows the normalized C-V characteristics of J2. The normalization procedure is similar to the technique used in Figures 5 through 13. It involves dividing the C-V characteristics after each measurement by the initial C-V characteristics. For example, the C-V characteristics measured after 200 hours of stress were divided by the C-V characteristics at 0 hours. Care was taken to normalize at the same voltage values. Changes from the initial conditions can be observed by comparing each measurement with the ratio of 1. Notice that Figure 15 shows a variation of less than 1%.

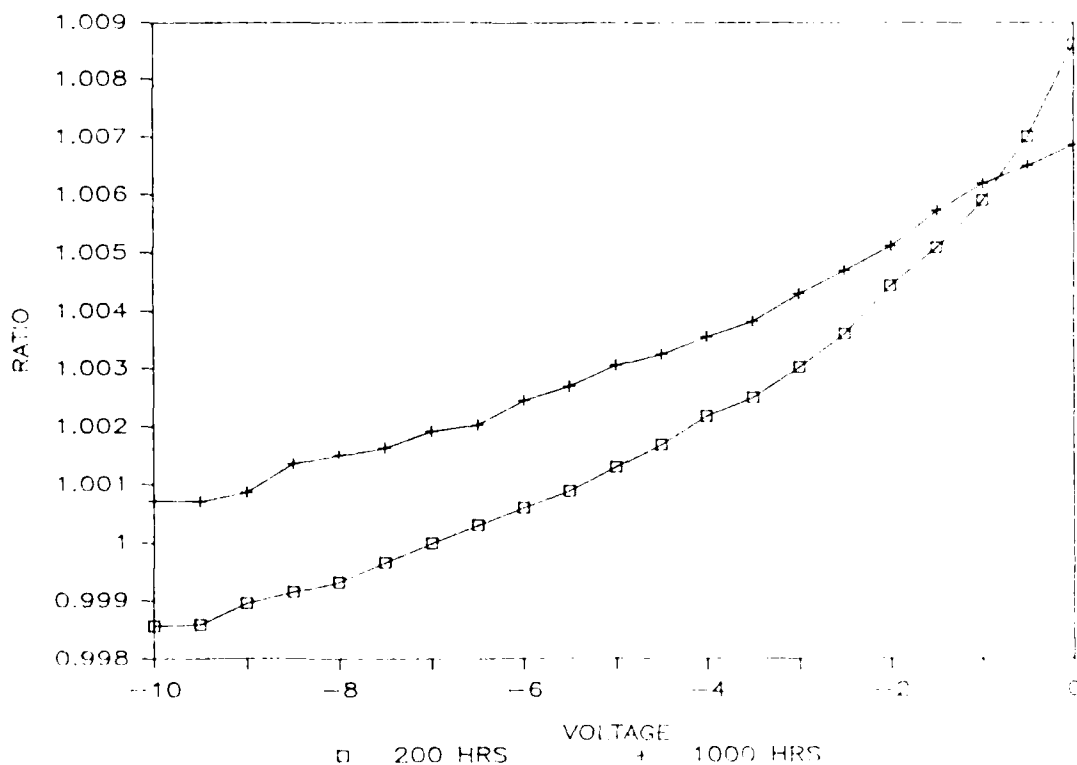


Figure 15. Normalized C-V Characteristics (J2)

Figure 16 shows the normalized C-V characteristics of X5, an IRED that exhibited a decrease in radiant power of 38% after 1000 hours of stress (Figure 12). Since the changes after stress did not exceed the changes displayed by the control IRED J2 in Figure 15, a relationship between the C-V characteristics and the radiant power degradation could not be determined. Analysis of other IREDS resulted in the same conclusion. Further research should include an automated system that can reduce the variability of the measurements by duplicating the measuring conditions more precisely and by obtaining average values.

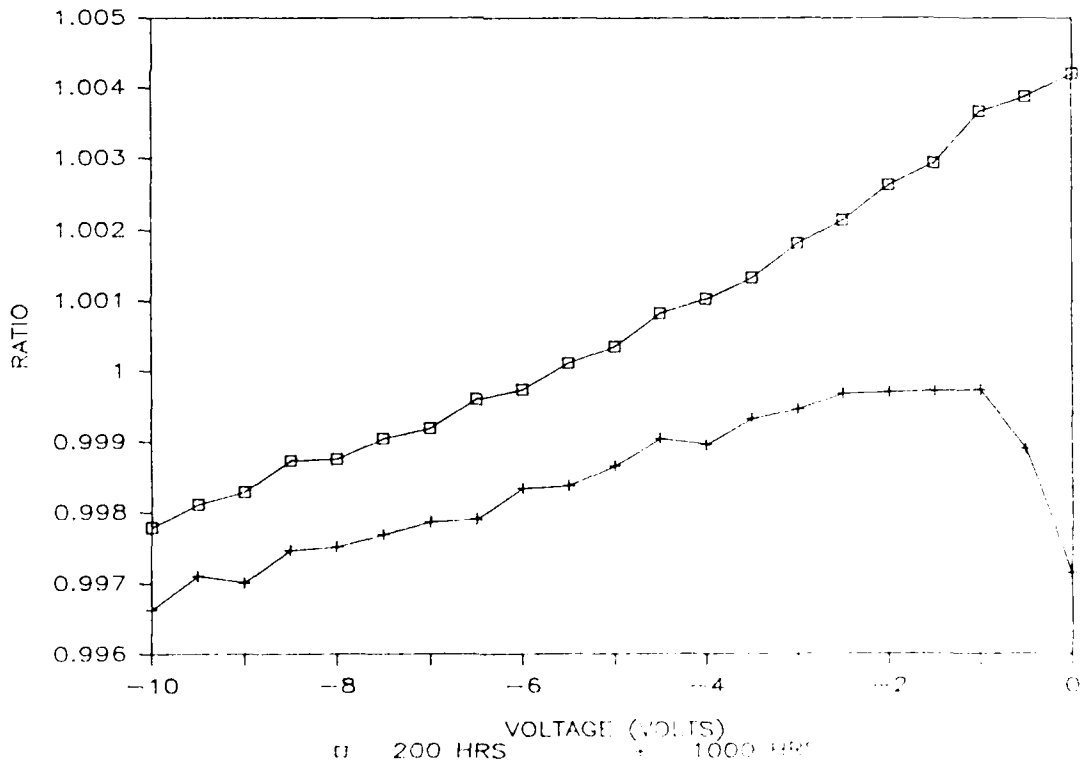


Figure 16. Normalized C-V Characteristics (X5)

Figure 17 shows the doping profile for J2. This profile resulted from the use of a FORTRAN program [APPENDIX I] that implemented Equation (11) from CHAPTER II, Part A. The profile indicates that at a junction width of approximately 0.6 microns, the doping concentration is about  $7E+15$  atoms/cm<sup>3</sup>. The concentration of donor and acceptor atoms is approximately equal, therefore, the junction extends an equal distance into the p-type and n-type regions. As the junction increases in width (due to an increase in the reverse bias), the doping concentration becomes greater. The result is a linearly-graded junction.

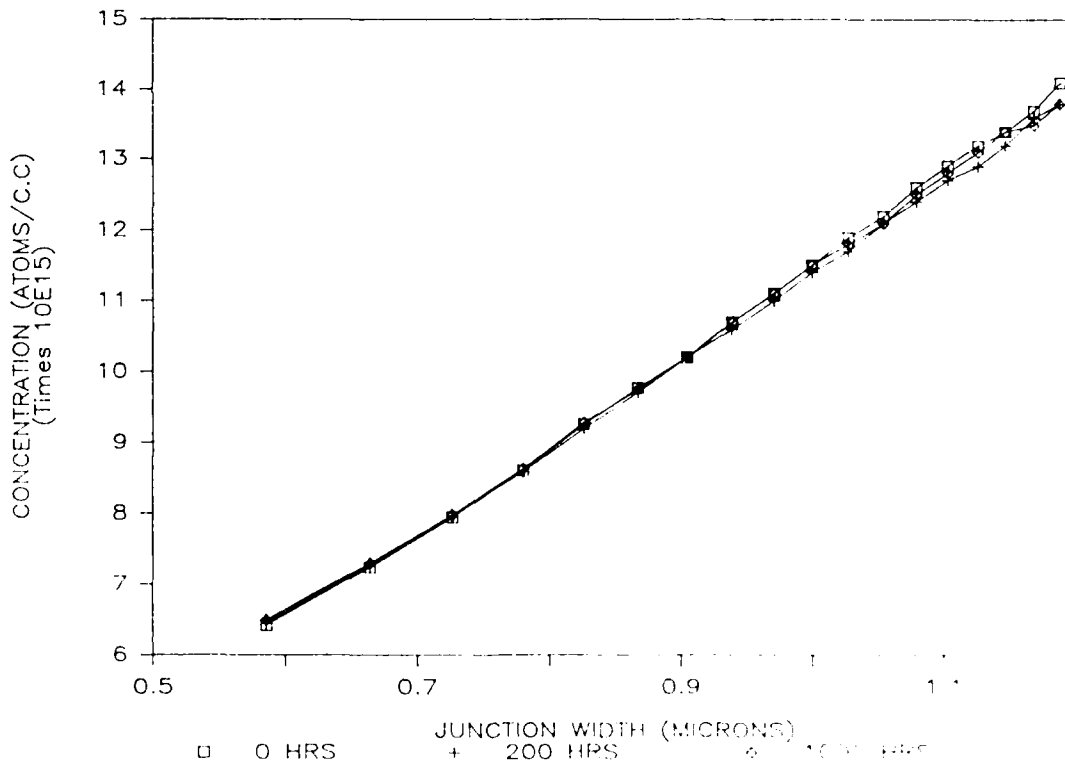


Figure 17. Doping Profile (J2)

Figure 18 shows the normalized doping profile for J2. Notice that the variation is about 2%.

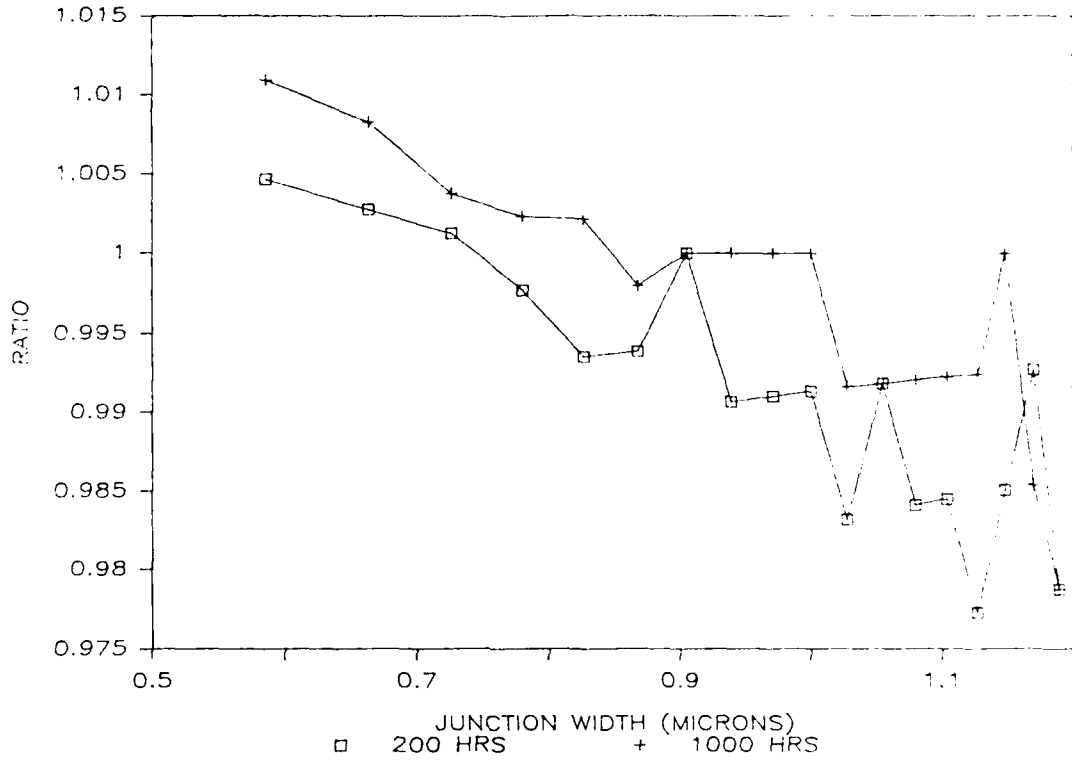


Figure 18. Normalized Doping Profile (J2)



Figure 19 shows the normalized doping profile for X5. Just as in Figure 16, the changes after stress do not exceed the changes in the control IRED J2 shown in Figure 18. Therefore, a relationship between the doping profile and the radiant power degradation shown in Figure 12 cannot be determined.

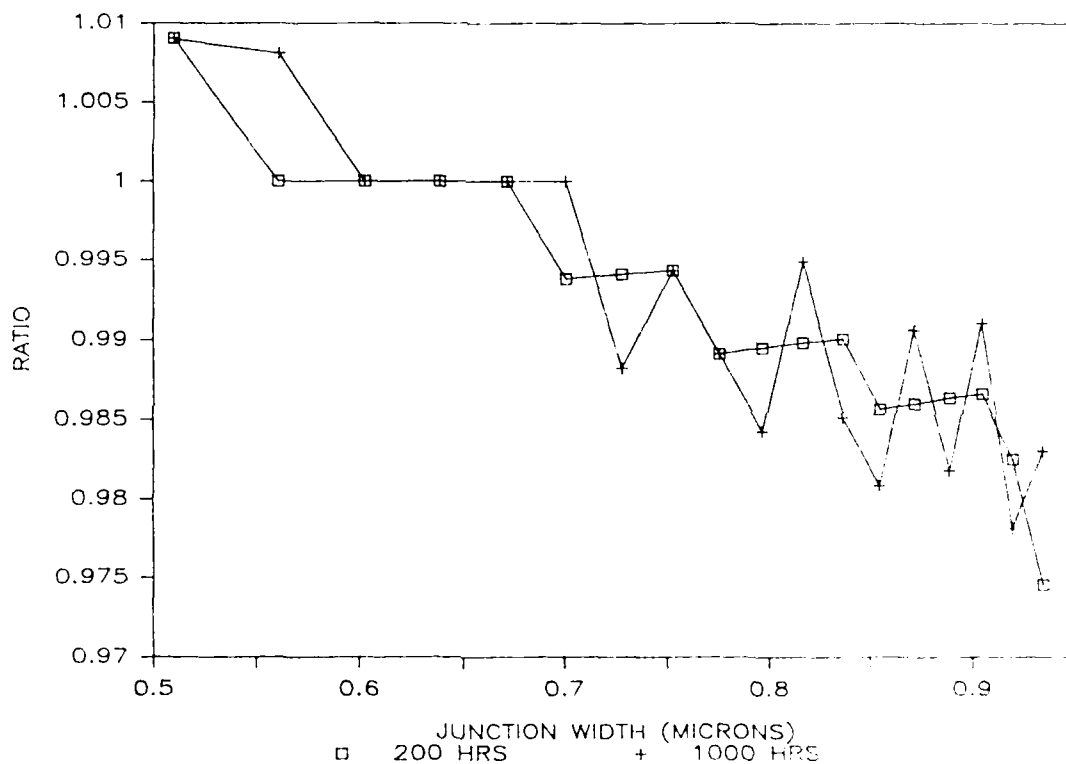


Figure 19. Normalized Doping Profile (X5)

Figure 20 shows the reverse I-V characteristics for J2. Notice the linearity that indicates an ohmic relationship between the reverse current and the reverse bias. The IREDS investigated in this work showed both a linear and an exponential relationship in the reverse I-V characteristics. The average breakdown voltage was approximately -30 volts.

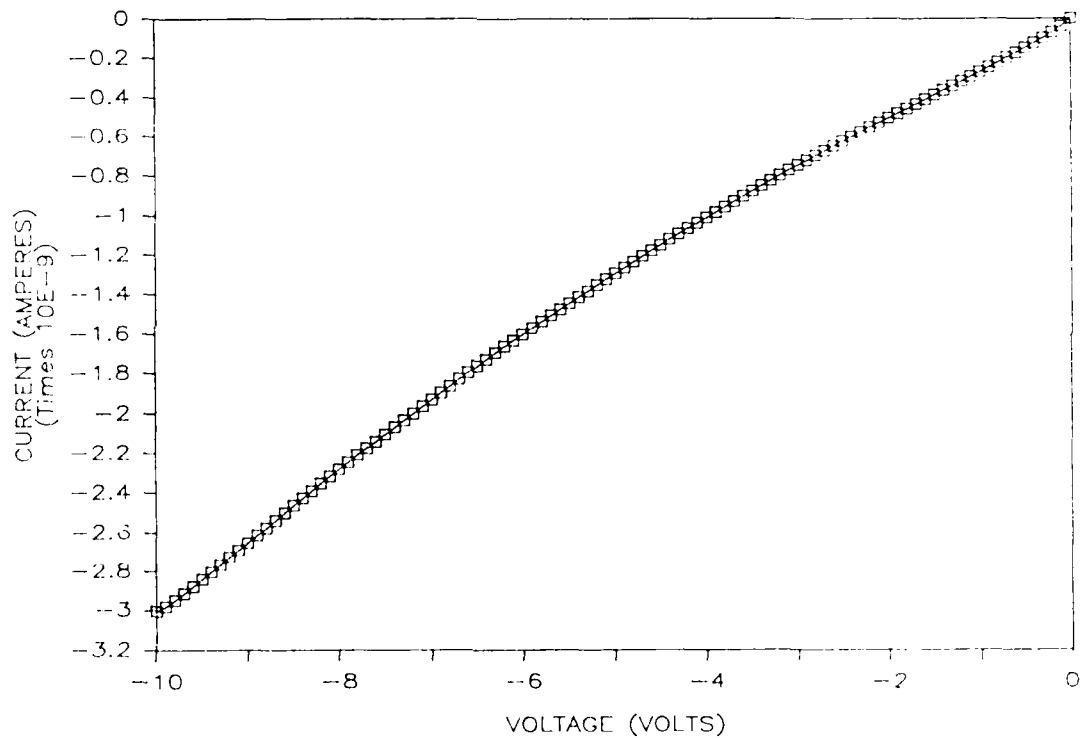


Figure 20. Reverse I-V Characteristics (J2)

Figure 21 shows the normalized reverse I-V characteristics of J2. Notice that the variation is less than 10%. Furthermore, the changes appear constant over the entire range of reverse bias.

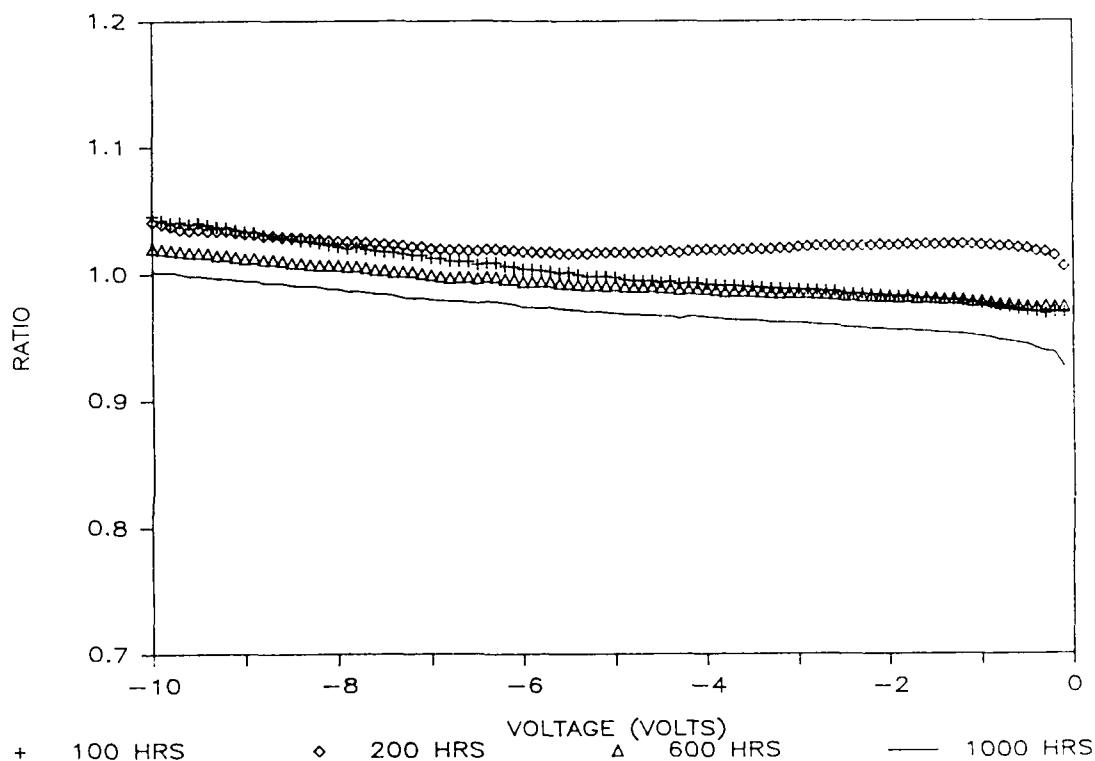


Figure 21. Normalized Reverse I-V Characteristics (J2)

Figure 22 shows the normalized reverse I-V characteristics of X5. The changes after stress exceed the changes displayed by the control IRED J2 shown in Figure 21. This indicates that there is a relationship between stress and the reverse I-V characteristics. Further analysis showed that virtually all of the stressed IREDs exhibited significant changes in their reverse I-V characteristics. However, the changes did not indicate a precise pattern, therefore, a relationship between the reverse I-V characteristics and the radiant power degradation was not determined.

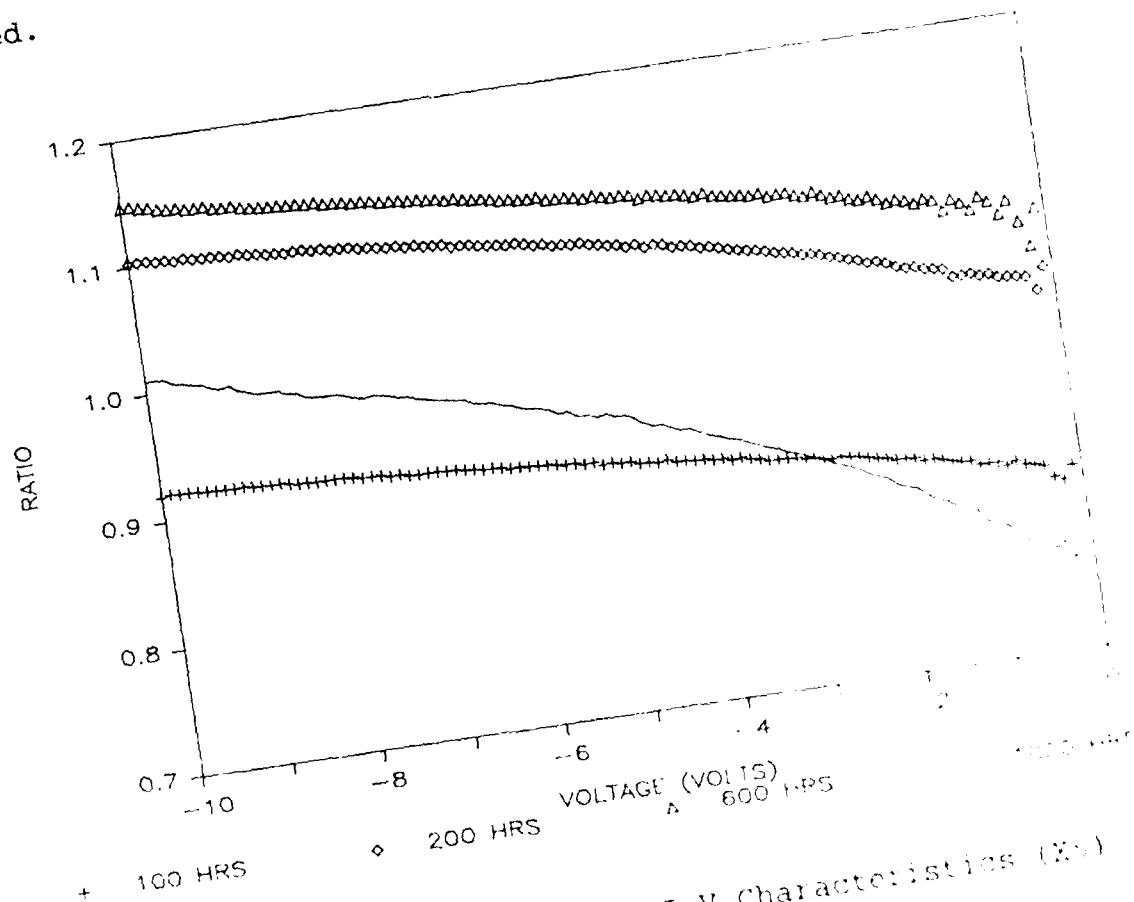


Figure 22 Normalized Reverse I-V Characteristics (X5)

Figure 23 shows the forward I-V characteristics for J2. Notice that the "turn-on" voltage is about 1 volt. This is a typical value for GaAs:Si IREDS. In contrast, GaAlAs:Si IREDS display a "turn-on" voltage of about 1.2 volts. Furthermore, the series resistance for most of the IREDS included in this work was about 3 ohms.

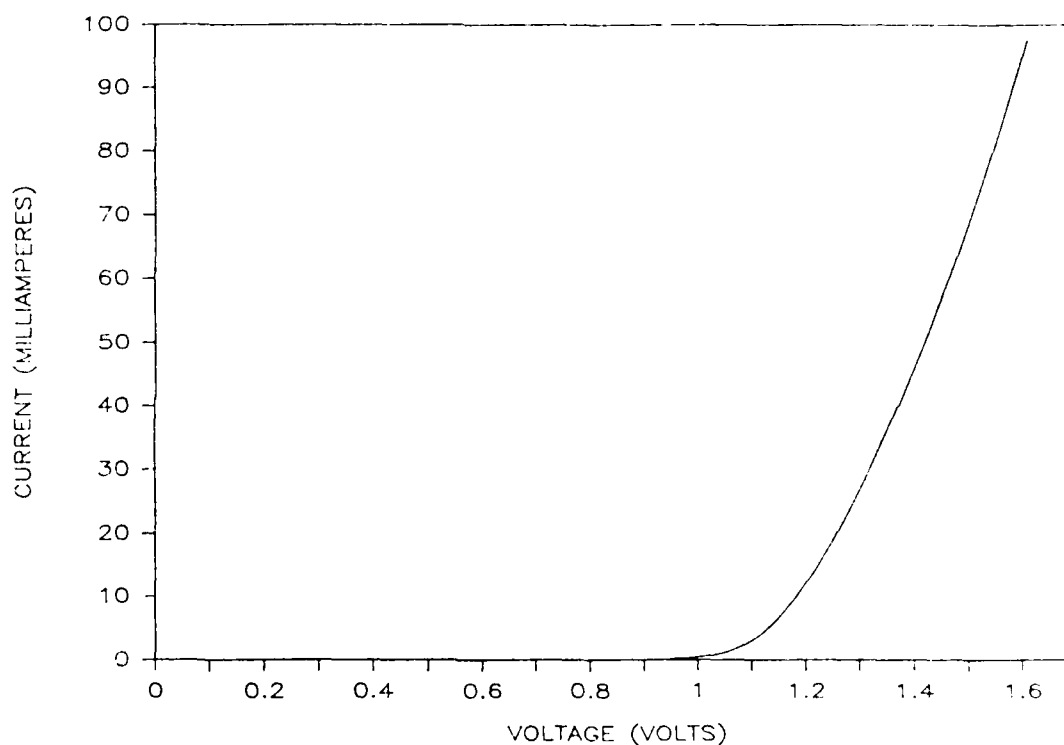


Figure 23. Forward I-V Characteristics (J2)

Figure 24 shows the normalized forward I-V characteristics for J2. Notice that the variation is about 10%. In addition, the variation appears in the region dominated by the recombination current. Further analysis showed that the variations corresponded to the changes exhibited by  $I_{RO}$  [Equation (17)] or "m", the recombination ideality factor. These changes could be due to variations in the measuring conditions or normal diode behavior. Also, notice that the currents at all measurement intervals converged at voltages above 1.4 volts. This is attributed to the series resistance of the IRED.

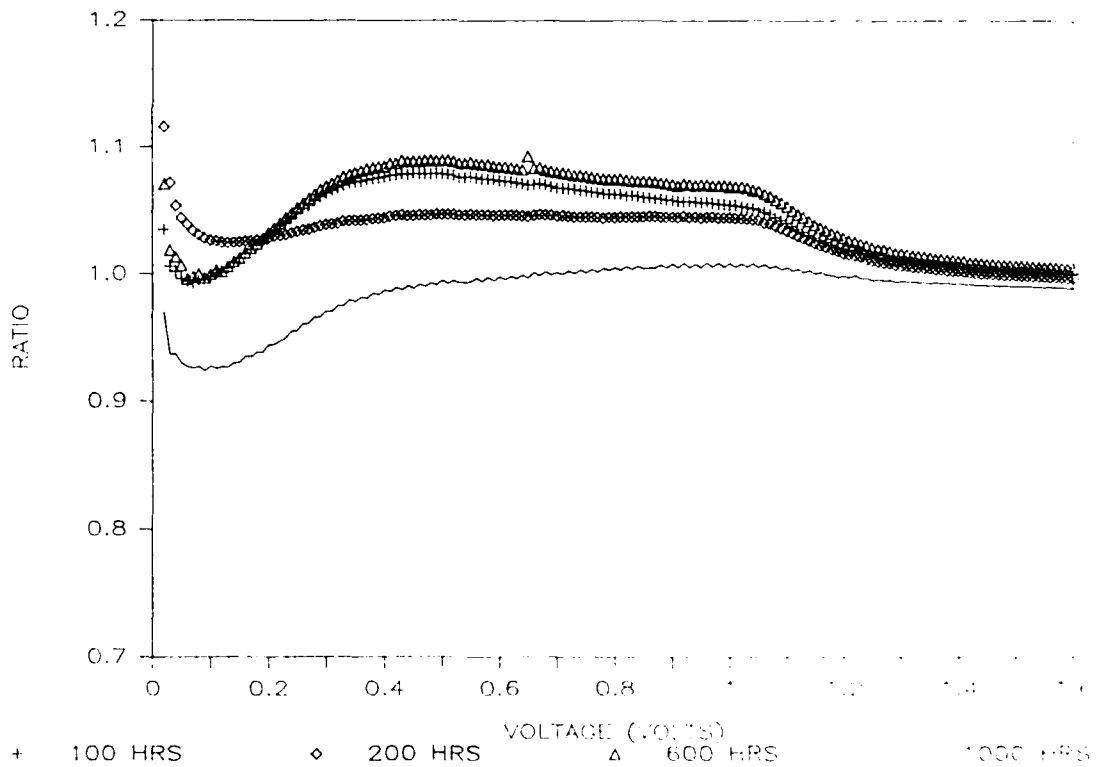


Figure 24. Normalized Forward I-V Characteristics (J2)

Figure 25 shows the normalized forward I-V characteristics of X5. Notice the changes that occur at about 1.2 volts. This is the region where the diffusion current dominates. Further analysis showed that virtually every stressed IRED exhibited this characteristic. However, just as in the reverse I-V characteristics, the changes did not show a precise pattern. Never-the-less, since radiant power is directly proportional to the diffusion current [Equation (28)], a relationship between the forward I-V characteristics and the radiant power degradation can be hypothesized.

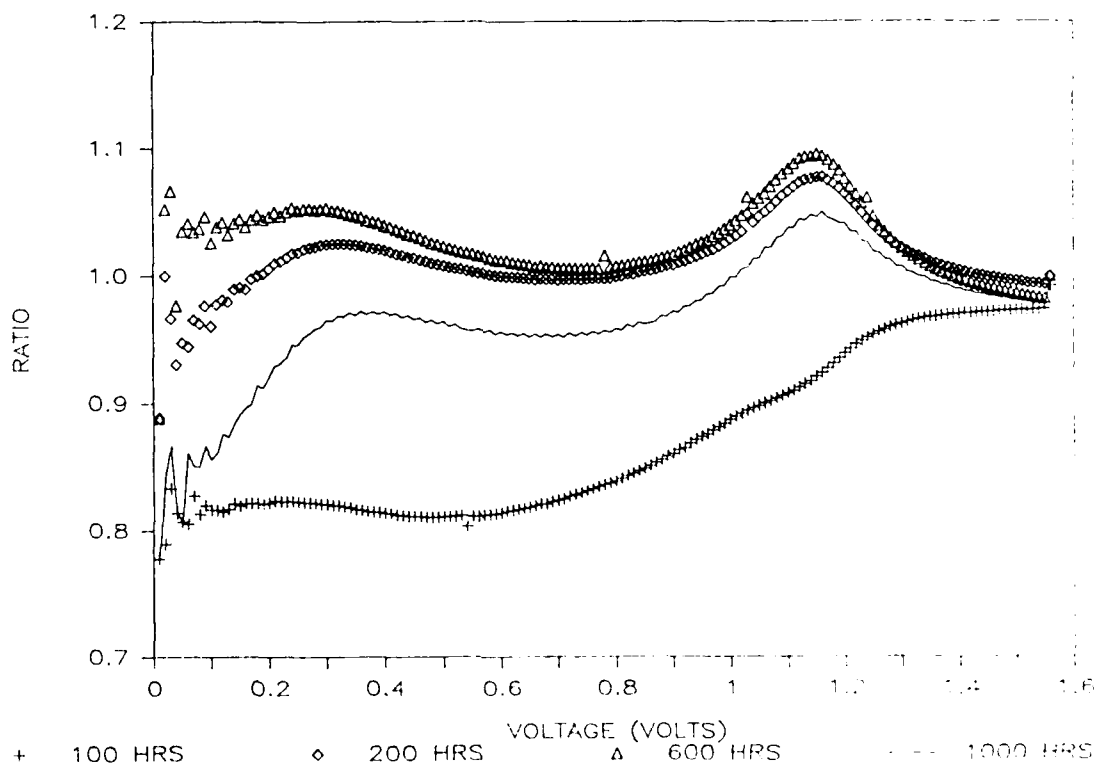


Figure 25. Normalized Forward I-V Characteristics (X5)

If the diffusion current increases and the radiant power decreases, Equation (28) states that the internal quantum efficiency ( $Q_i$ ) must decrease (assuming the effective wavelength of the emitted photon remains constant). Figure 26 shows the normalized internal quantum efficiency as a function of time for IREDS X5-X8. This graph was produced using Equation (41) from CHAPTER II, Part D. Notice the similarities between Figures 12 and 26. This indicates that the increase in the diffusion current is non-radiative. Thus, the radiant power degradation is attributed to a decrease in the IRED internal quantum efficiency.

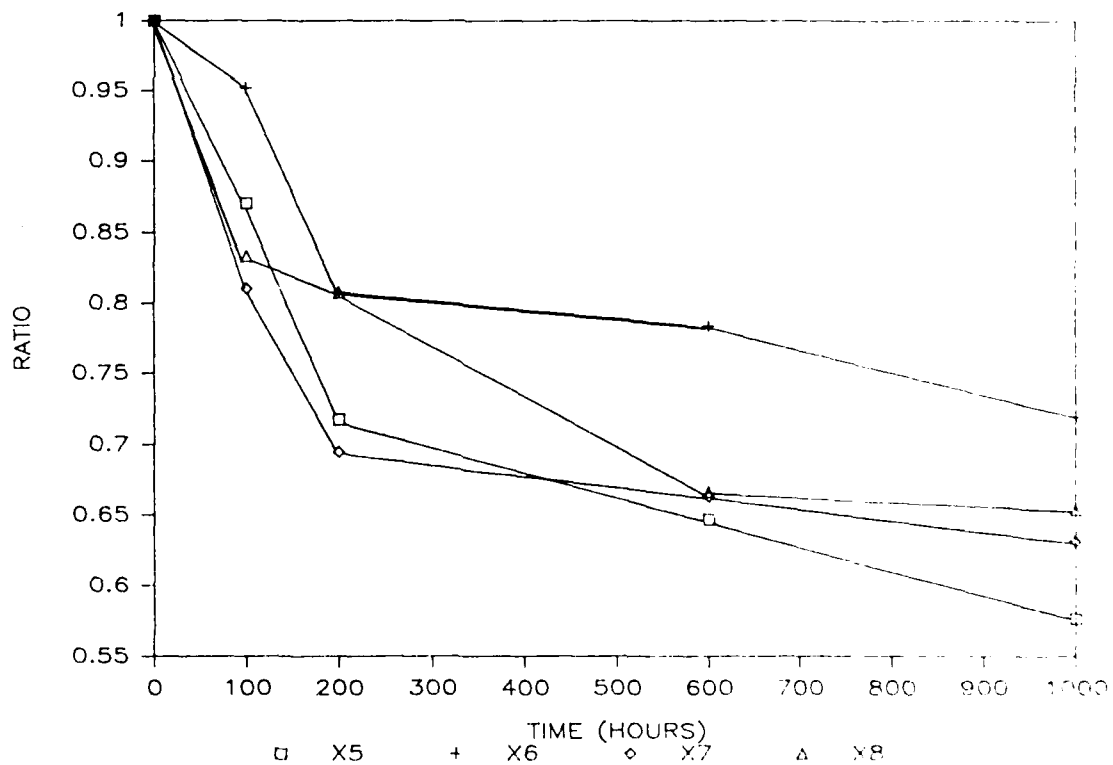


Figure 26. Normalized  $Q_i$  vs Time (X5-X8)



The most dramatic change in the reverse I-V characteristics of any stressed IRED in this work was displayed by X4 between 600 and 1000 hours of stress. This change is shown in Figure 27.

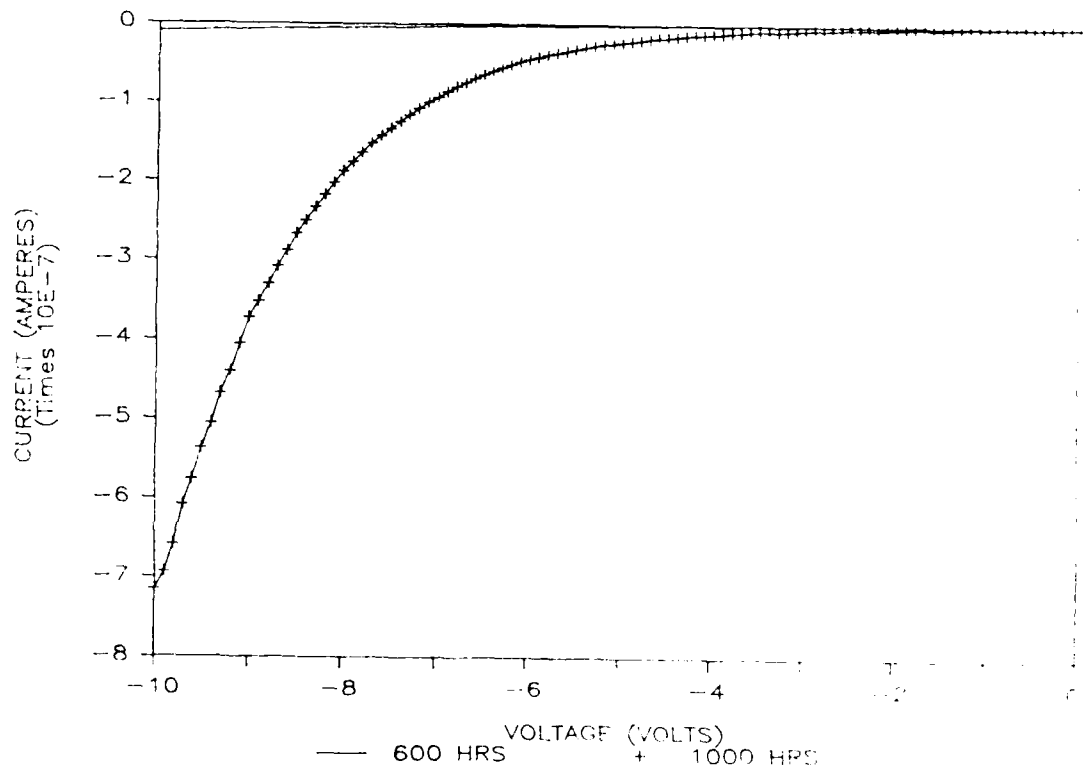


Figure 27. Reverse I-V Characteristics (X4)

Figure 28 shows the normalized reverse I-V characteristics of X4. Although the change is undoubtedly due to stress, a link to the radiant power degradation in Figure 11 is not clear. From Figure 11, notice that the degradation after 600 hours shows a ratio of about 0.94 whereas the degradation after 1000 hours shows a ratio of 0.90.

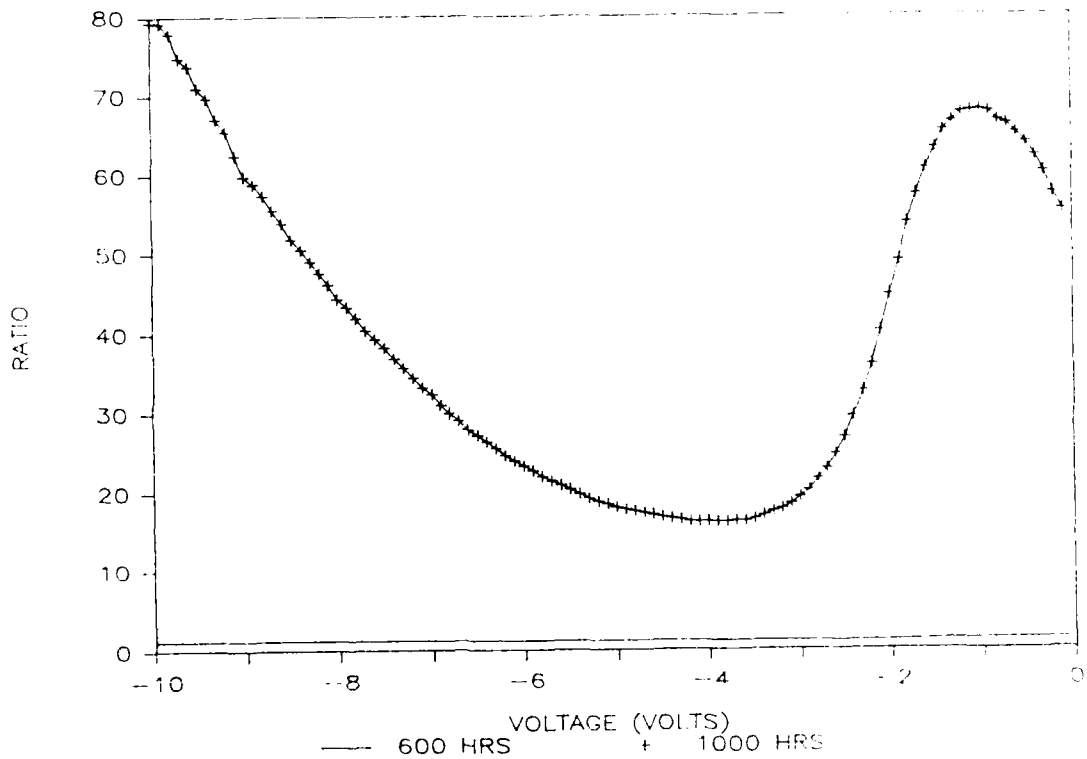


Figure 28. Normalized Reverse I-V Characteristics (X4)

Figure 29 shows the reverse I-V characteristics as a function of temperature for X4. The voltage and current values displayed by the CURSOR correspond to the 25°C line. The values displayed by the MARKER correspond to the 75°C line. A comparison of these values shows that the reverse current increases by a factor of 3 with a 50°C rise in temperature. This small increase indicates that the reverse current mechanism is the generation of electron-hole pairs in the space-charge region. The control IREDS also showed this relationship. Thus, stress changes the magnitude and not the mechanism of the reverse current.

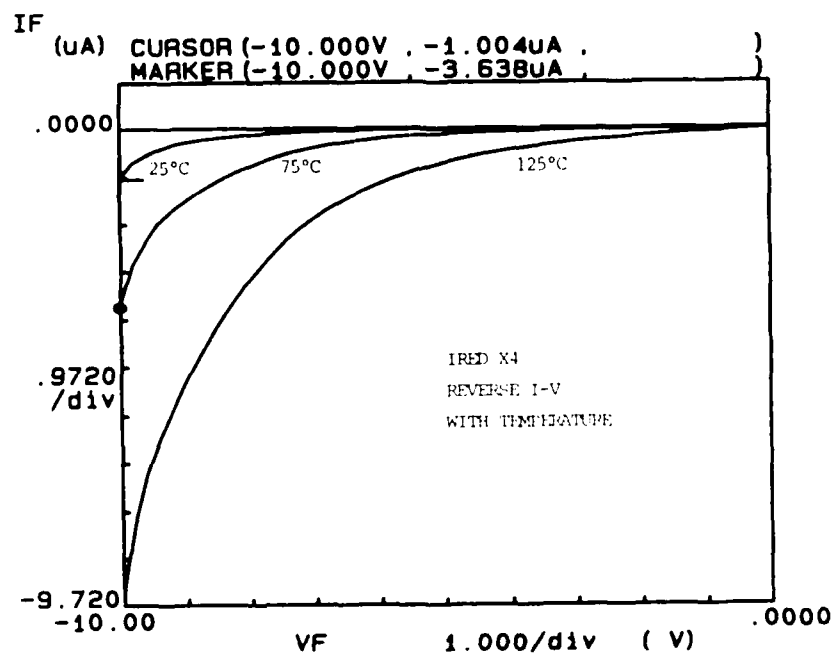


Figure 29. Reverse I-V Characteristics (X4)

Figure 30 shows the forward I-V characteristics of X4 after 600 and 1000 hours of stress. This illustrates that the dramatic change that occurs in the reverse I-V characteristics also appears in the forward I-V characteristics.

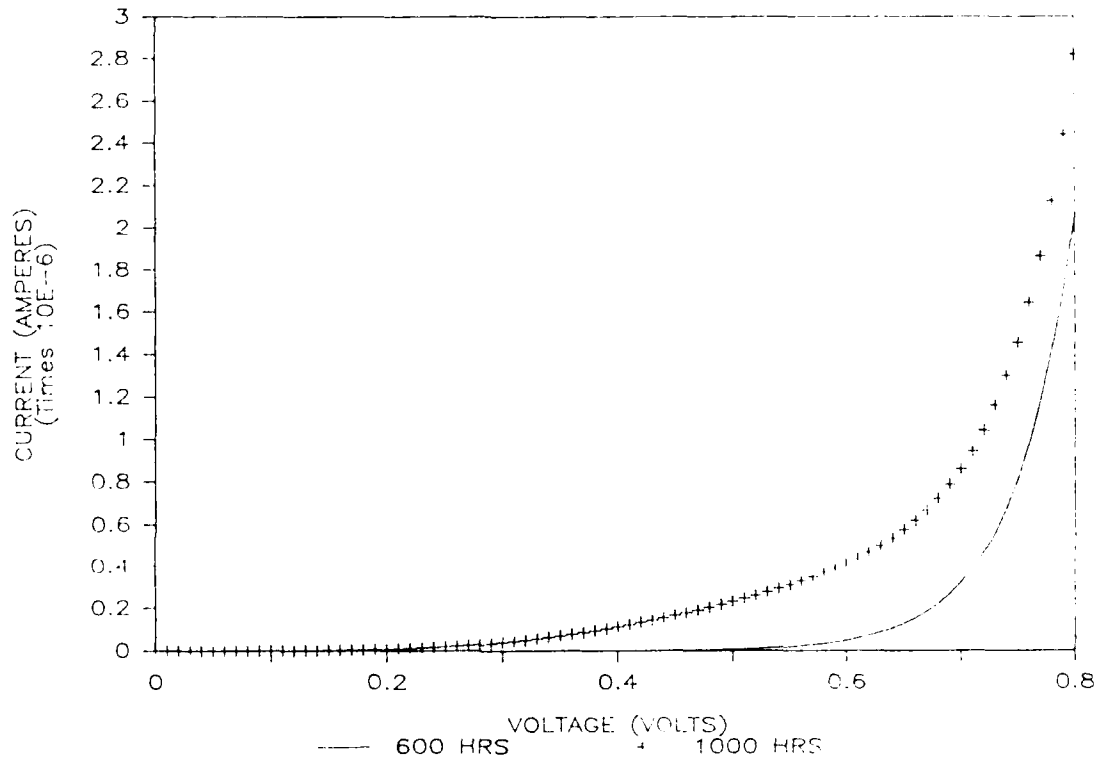


Figure 30. Forward I-V Characteristics (X4)

Figure 31 shows the forward log I-V characteristics of X4 after 600 and 1000 hours of stress. Notice that the change after 1000 hours dominates the recombination current below 0.8 volts.

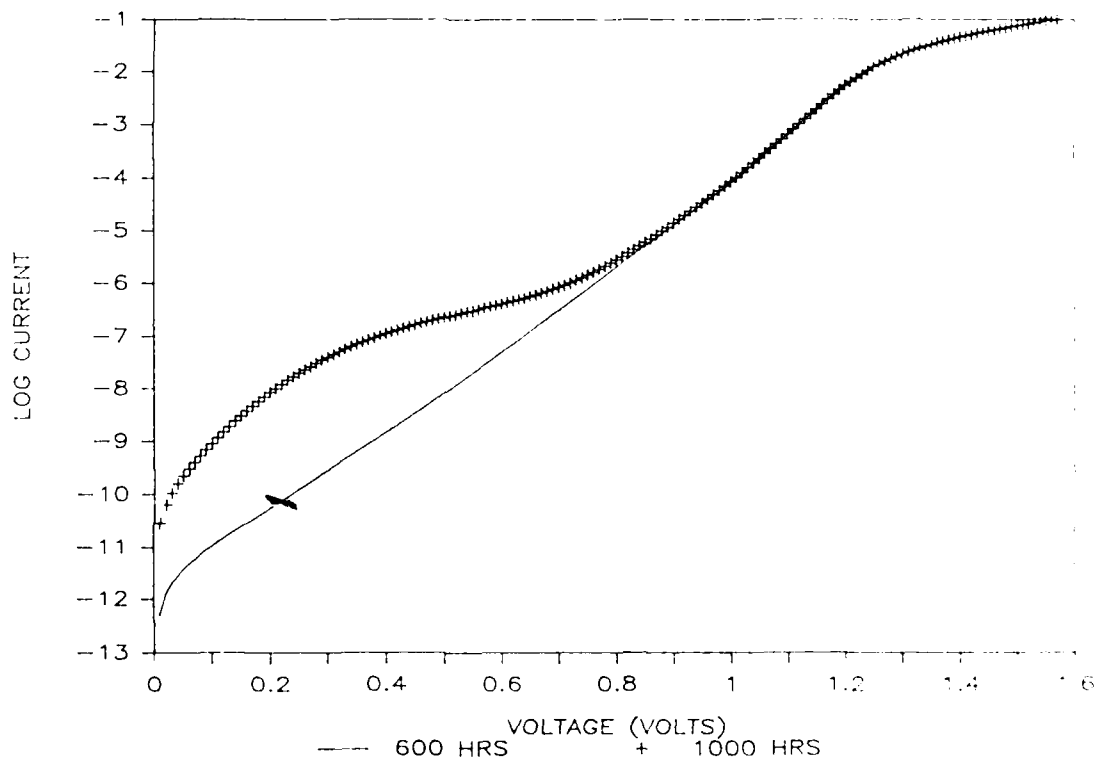


Figure 31. Forward Log I-V Characteristics (X4)

Figure 32 shows the forward log I-V characteristics as a function of temperature for X4. Notice that the current at low voltages does not display the same temperature dependence as the recombination current. This is evidenced by the merging of the two current components at 175°C.

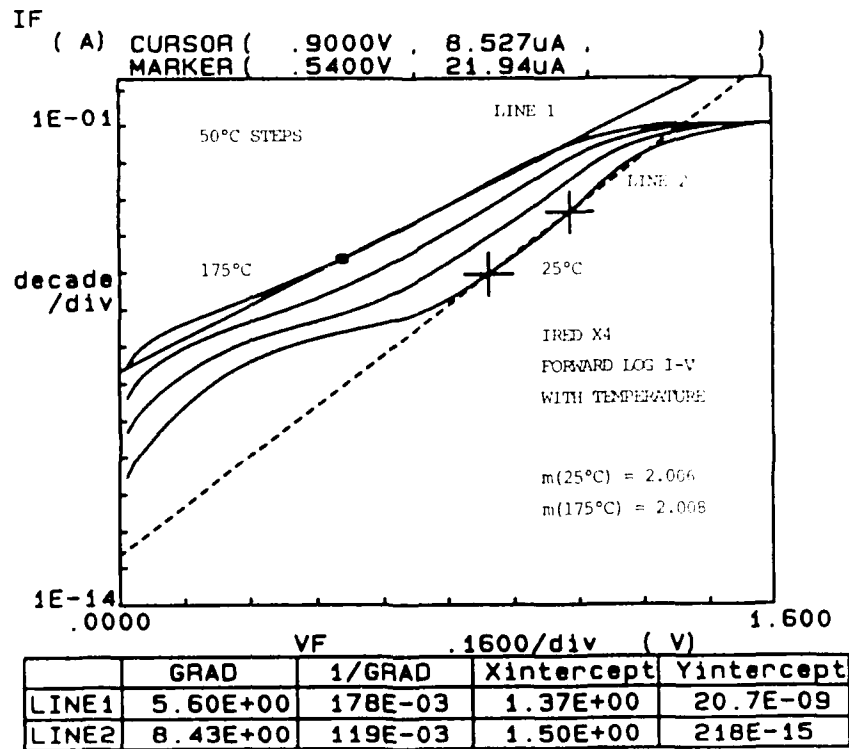


Figure 32. Forward Log I-V Characteristics w/Temp (X4)

Figure 33 shows the forward log I - log V characteristics of X4 after 600 and 1000 hours of stress. Notice the 1000 HRS data corresponding to the region near the -0.4 LOG VOLTAGE point. The linearity in this region indicates a power relationship between the forward current and the forward voltage.

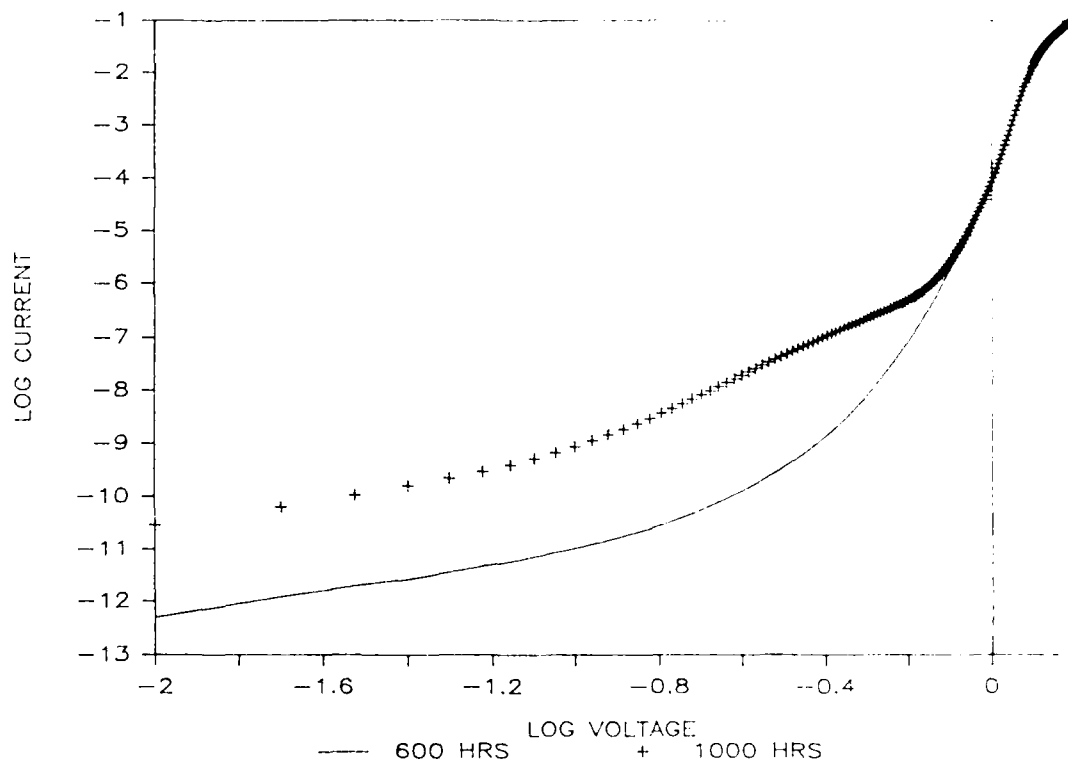


Figure 33. Forward Log I - Log V Characteristics (X4)

## CHAPTER V

### SUMMARY

This work measured the C-V, I-V, and P-I-V diode characteristics of GaAs:Si and GaAlAs:Si IREDS that exhibited radiant power degradation with stress. Normalization graphs that compared initial conditions with periodic measurements of stressed and unstressed IRED characteristics provided excellent techniques for analyzing changes in the characteristics with time. In addition, the unstressed diodes served as reliable gauges of the variability of the measuring system.

A general theory concerning radiant power degradation presented itself due to the extreme changes in the reverse and forward I-V characteristics with stress. The magnitude of the generation current was changed in almost every stressed IRED. A corresponding change was also displayed at low voltages in the recombination current. An increase in the diffusion current was observed in virtually every stressed IRED. Since the radiant power degraded, the increase in the diffusion current was assumed to be non-radiative. Thus, the radiant power degradation is attributed to a decrease in the internal quantum efficiency.

Although the GaAlAs:Si IRED C-V characteristics showed some changes, it was determined that the precision of the measuring system could not clearly indicate the changes.



## REFERENCES

1. J. Millman, Microelectronics, McGraw-Hill Book Company, New York, 1979.
2. B. G. Streetman, Solid State Electronic Devices, Prentice-Hall, Inc., Englewood Cliffs, N. J., 1980.
3. J. I. Pankove, Optical Processes in Semiconductors, Prentice-Hall, Inc., Englewood Cliffs, N. J., 1971.
4. J. Wilson and J. F. B. Hawkes, Optoelectronics: An Introduction, Prentice/Hall International, Englewood Cliffs, N. J., 1983.
5. H. Kressel and J. K. Butler, Semiconductor Lasers and Heterojunction LEDs, Academic Press, New York, 1977.
6. A. S. Grove, Physics and Technology of Semiconductor Devices, John Wiley and Sons, Inc., New York, 1967.
7. Hewlett-Packard Model 4280A Operation and Service Manual, 1983.
8. Hewlett-Packard Model 16058A Test Fixture Operating Note, 1983.
9. Delta Design Model 2300 Instruction Manual.
10. Hewlett-Packard Model 4145A Semiconductor Parameter Analyzer Operation and Service Manual, 1984.
11. United Detector Technology Model 61AC Operating Instruction Manual, 1986.
12. M. G. Craford, "Light-Emitting Diode Displays," from Flat-Panel Displays and CRTs, edited by L. E. Tannas, Jr., Van Nostrand Reinhold Co., New York, 1985.
13. C. Van Opdorp and L. Blok, "Simple Method for Accurately Determining the Injection Efficiency and Bulk Quantum Efficiency of Light-Emitting Diodes," Solid-State Electronics, Vol. 25, No. 7, pp. 599-610, 1982.
14. Honeywell Optoelectronics Data Book, 1986.
15. TRW Optoelectronics Data Book, 1985.
16. J. D. Spencer and D. E. Pippenger, The Voltage Regulator Handbook, Texas Instruments, Dallas, Tex., 1977.

## APPENDIX I

```

C THIS PROGRAM CALCULATES THE DOPING CONCENTRATION OF A DIODE AS A
C FUNCTION OF JUNCTION WIDTH. IT REQUIRES 22 POINTS FROM THE Q-V
C CHARACTERISTICS. THE PROGRAM WILL PROMPT YOU FOR THE NAME OF THE Q-V
C FILE AT RUNTIME.
      REAL*8 VOLTCAP(22,2),C(22),DERIV(22),WIDTH(22),DENSITY(22)
      REAL*8 KS,E0,Q,A
      READ(1,1)((VOLTCAP(I,J),J=1,2),I=1,22)
1     FORMAT(F10.5,E22.4)
C KS IS THE DIELECTRIC CONSTANT OF THE MATERIAL.
      KS=12.0D0
C E0 IS THE PERMITTIVITY OF FREE SPACE.
      E0=8.854D-14
C Q IS THE ELECTRONIC CHARGE.
      Q=1.602D-19
C A IS THE JUNCTION AREA.
      A=6.45D-4
C THIS DO LOOP FINDS THE RECIPROCAL OF CAPACITANCE SQUARED.
      DO 10 I=1,22
          C(I)=1.0D0/(VOLTCAP(I,1)+VOLTCAP(I,2))
10     CONTINUE
C THIS DO LOOP DIFFERENTIATES THE RECIPROCAL OF CAPACITANCE SQUARED.
      DO 20 I=3,20
          J=I+2
          K=I+1
          L=I-1
          M=I-2
          DERIV(I)=DABS((-1.0D0*C(J)+8.0D0*C(K)-8.0D0*C(L)+C(M))/5.0D0)
20     CONTINUE
C THIS DO LOOP COMPUTES THE WIDTH OF THE JUNCTION IN MICRONS FROM THE
C EQUATION THAT DESCRIBES THE JUNCTION AS A PARALLEL-PLATE CAPACITOR.
      DO 30 I=3,20
          WIDTH(I)=(A+KS+E0/VOLTCAP(I,2))+1.0D+4
30     CONTINUE
C THIS DO LOOP CALCULATES THE DOPING CONCENTRATION.
      DO 40 I=3,20
          DENSITY(I)=(2.0D0/(A+Q*KS+E0))+1.0D0/DERIV(I)
40     CONTINUE
C THIS DO LOOP WRITES THE WIDTH AND DOPING CONCENTRATION TO A FILE. THE
C PROGRAM WILL PROMPT YOU FOR A NAME AT RUNTIME.
      DO 50 I=3,20
          WRITE(2,60)WIDTH(I),DENSITY(I)
50     CONTINUE
50     FORMAT(1X,F8.3,E12.3)
      STOP
      END

```

## APPENDIX II

### GaAs INTRINSIC CARRIER CONCENTRATION CALCULATIONS

The intrinsic carrier concentration ( $N_i$ ) for GaAs is  
[2, Page 76]

$$N_i = (N_C N_V)^{1/2} \exp(-E_g/2eV_t) \quad (2.1)$$

where

$N_C$  = the effective density of states in the  
conduction band ( $\text{cm}^{-3}$ )

$N_V$  = the effective density of states in the valence  
band ( $\text{cm}^{-3}$ )

$E_g$  = the energy gap of the material  
= 1.41 eV for GaAs

$e$  = the electron

$V_t$  = the voltage equivalent of temperature (volts)  
= the temperature in degrees Kelvin  
11601

The effective density of states in the conduction band  
( $N_C$ ) is [2, Page 75]

$$N_C = 2[2(\pi) m_n k T/h^2]^{3/2} \quad (2.2)$$

where

$\pi$  = 3.1415927

$m_n$  = the electron effective mass (kg)

$k$  = Boltzmann's constant  
=  $1.38\text{E}-23 \text{ J}/^\circ\text{K}$

T = the temperature ( $^{\circ}\text{K}$ )

h = Planck's constant

$$= 6.63\text{E-}34 \text{ J-sec}$$

The effective mass of the electron ( $m_n$ ) for GaAs is  
[5, Page 17]

$$m_n = .068 m_o \quad (2.3)$$

where

$$\begin{aligned} m_o &= \text{the mass of the electron} \\ &= 9.11\text{E-}31 \text{ kg} \end{aligned} \quad (2.4)$$

Substitution of (2.4) in (2.3) gives

$$m_n = 6.20\text{E-}32 \text{ kg} \quad (2.5)$$

Substitution of (2.5) and the appropriate constant values  
in (2.2) gives

$$N_c = 8.55\text{E+}13 T^{3/2} \text{ cm}^{-3} \quad (2.6)$$

The effective density of states in the valence band  
( $N_v$ ) is [2, Page 75]

$$N_v = 2[2(\pi) m_p k T/h^2]^{3/2} \quad (2.7)$$

where

$$\begin{aligned}
m_p &= \text{the hole effective mass (kg)} \\
&= .47m_0 \text{ for GaAs [5, Page 22]} \\
&= 4.28E-31 \text{ kg} \qquad (2.8)
\end{aligned}$$

Substitution of (2.8) and the appropriate constant values in (2.7) gives

$$N_v = 1.55E+15 T^{3/2} \text{ cm}^{-3} \qquad (2.9)$$

Substitution of (2.6), (2.9), and  $E_g = 1.41 \text{ eV}$  for GaAs in (2.1) gives

$$N_i = (3.64E+16)T^{3/2} \exp[-(8178.71)/T] \qquad (2.10)$$

Using (2.10), the values for  $N_i$  at various temperatures are calculated as follows:

$$\begin{aligned}
N_i(25^\circ\text{C} = 298^\circ\text{K}) &= 2.3E+8 \text{ cm}^{-3} \\
N_i(75^\circ\text{C} = 348^\circ\text{K}) &= 1.5E+10 \text{ cm}^{-3} \\
N_i(125^\circ\text{C} = 398^\circ\text{K}) &= 3.4E+11 \text{ cm}^{-3} \\
N_i(175^\circ\text{C} = 448^\circ\text{K}) &= 4.1E+12 \text{ cm}^{-3}
\end{aligned}$$

APPENDIX III  
MEASURING RADIANT POWER

1. The equipment is described in CHAPTER III, Part C.
2. Place the diode to be tested in the opening of the integrating sphere. Be sure both the integrating sphere and the diode are stationary.
3. Check the optometer. Be sure the CH 1 button is pushed. Push the CAL TEST button. The display should read .152. If it does not, use a small screwdriver to change the CAL ADJ 1 button on the back of the optometer. Once it reads .152, release the CAL TEST button.
4. Push the ZERO AUTO MAN button. Turn the MULTIPLIER dial to  $10^3$ . Push the ZERO SET button. Once the display reads .000, release the ZERO SET button. Do not release the ZERO AUTO MAN button. Turn the MULTIPLIER dial slowly to  $10^{-2}$ . (You have now compensated the optometer for ambient light). The display may still read something on the  $10^{-2}$  MULTIPLIER setting. If it does, consider it an offset that must be subtracted from your measurements. The  $10^{-2}$  MULTIPLIER setting is equivalent to microwatts. For example, if the display reads .123, the value is .123E-5, or 1.23E-6 watts. Each change of the MULTIPLIER dial multiplies the display by 10.

5. Set the HP4145 to input a current or voltage. This can be done using pages 3-34 through 3-41 of the HP4145 Operating Manual. It is important to enter 6 seconds DELAY TIME. Use page 3-45 to setup the LIST DISPLAY.
6. At the appropriate time, push the SINGLE MEASUREMENT button on the HP4145. If the DELAY TIME has been set to 6 seconds, you will have that long to record the optometer reading. If you sweep a current or voltage with the HP4145, you will have 6 seconds to record each optometer reading. At the end of the sweep, record the current and voltage readings from the HP4145. It would be very helpful to automate this measurement system.
7. Once the radiant power measurements are finished for one diode, steps 2 through 6 must be repeated for any successive diodes.

## APPENDIX IV

### HEAT SINK DESIGN

The maximum power dissipation of a semiconductor is determined by the maximum junction temperature at which the device will operate and the device's ability to dissipate heat generated internally. [16, Page 39] Power dissipation ( $P_d$ ) may be expressed as

$$P_d = \frac{T_j - T_a}{R_{jC} + R_{Ca}} \quad (4.1)$$

where

$T_j$  = the junction temperature ( $^{\circ}\text{C}$ )

$T_a$  = the ambient temperature ( $^{\circ}\text{C}$ )

$R_{jC}$  = the junction-to-case thermal resistance ( $^{\circ}\text{C}/\text{W}$ )

$R_{Ca}$  = the case-to-ambient thermal resistance ( $^{\circ}\text{C}/\text{W}$ )

The goal of power dissipation is to maximize  $P_d$  while keeping  $T_j$  below the maximum allowable junction temperature provided by the manufacturer's data sheets. The junction-to-case thermal resistance is a fixed parameter that is also provided by the manufacturer's data sheets. The ambient temperature ( $T_a$ ) can be controlled, but it often requires expensive equipment. Therefore, the best approach to increase the power dissipation is to decrease the case-to-ambient thermal resistance ( $R_{Ca}$ ). This is the purpose of heat sink design.



An expression describing  $R_{Ca}$  is

$$R_{Ca} = R_{CS} + \frac{1}{Ag(F_C H_C + e H_r)} \quad (4.2)$$

where

$R_{CS}$  = the case-to-heat sink thermal resistance ( $^{\circ}\text{C}/\text{W}$ )

$A$  = the surface area of the heat sink ( $\text{in}^2$ )

$g$  = the effectiveness of the heat sink

$F_C$  = the convection current factor

$H_C$  = the convection heat transfer coefficient  
( $\text{W}/\text{in}^2\text{-}^{\circ}\text{C}$ )

$e$  = the emissivity of the heat sink material

$H_r$  = the normalized radiation heat transfer coefficient  
( $\text{W}/\text{in}^2\text{-}^{\circ}\text{C}$ )

The case-to-heat sink thermal resistance is approximately-  
 $3^{\circ}\text{C}/\text{W}$  if a heat sink compound is not used. Archer Heat  
Sink Compound can lower  $R_{CS}$  to about  $1^{\circ}\text{C}/\text{W}$ , but this  
is not a significant change, so

$$R_{CS} = 3^{\circ}\text{C}/\text{W} \quad (4.3)$$

The surface area is

$$A = 5.29 \text{ in}^2 \quad (4.4)$$

From Table 5.8, page 52 [16], for vertical rectangular  
plane,

$$L = \text{Height} = 1 \text{ inch} \quad (4.5)$$

From Figure 5.6, page 53 [16], for  $(T_S - T_a) = 40^\circ\text{C}$ ,

$$H_C = 5.5\text{E-}3 \text{ W/in}^2\text{-}^\circ\text{C} \quad (4.6)$$

From Table 5.9, page 53 [16], for vertical plane,

$$F_C = 1.0 \quad (4.7)$$

From Figure 5.7, page 54 [16], for  $(T_S - T_a) = 40^\circ\text{C}$ ,

$$H_r = .45\text{E-}2 \text{ W/in}^2\text{-}^\circ\text{C} \quad (4.8)$$

From Table 5.10, page 55 [16], for polished aluminum,

$$e = 0.15 \quad (4.9)$$

From 1, page 55 [16],

$$hT = F_C H_C + e H_r \quad (4.10)$$

$$hT = 6.175\text{E-}3 \text{ W/in}^2\text{-}^\circ\text{C} \quad (4.11)$$

From Figure 5.9, page 56 [16], for fin thickness of .625 in.,

$$g > 94\% \quad (4.12)$$

assume

$$g = 1.0 \quad (4.13)$$

Thus,

$$R_{Ca} = 3 + \frac{1}{(5.29)(1.0)(6.175\text{E-}3)} \quad (4.14)$$

$$R_{Ca} = 34^\circ\text{C/W} \quad (4.15)$$

APPENDIX V  
JUNCTION TEMPERATURE CALCULATIONS

The junction temperature ( $T_j$ ) is [16, Page 39]

$$T_j = (R_{jC} + R_{cA}) P_d + T_a \quad (5.1)$$

where

$R_{jC}$  = the junction-to-case thermal resistance ( $^{\circ}\text{C}/\text{W}$ )

$R_{cA}$  = the case-to-ambient thermal resistance ( $^{\circ}\text{C}/\text{W}$ )

$P_d$  = the power dissipated in the material (W)

$T_a$  = the ambient temperature ( $^{\circ}\text{C}$ )

The junction-to-case thermal resistance ( $R_{jC}$ ) is a function of the IRED package. The IREDs tested in this work used a metal TO-46 package. The thermal resistance for TO-46 is typically  $100^{\circ}\text{C}/\text{W}$  to  $150^{\circ}\text{C}/\text{W}$ . [14, Page 225] For the purposes of this work, the worse case was used, so

$$R_{jC} = 150^{\circ}\text{C}/\text{W} \quad (5.2)$$

From APPENDIX IV,

$$R_{cA} = 34^{\circ}\text{C}/\text{W} \quad (5.3)$$

The power dissipated ( $P_d$ ) in the material is

$$P_d = I_F V \quad (5.4)$$

where

LIST OF TABLES

Table	Page
1. Intrinsic Carrier Concentration for GaAs.....	7
2. IRED Stressing Conditions.....	24

CHAPTER I  
INTRODUCTION

Infrared light-emitting diodes (IREDS) have many important applications including guidance and communication systems. These applications are often in remote areas such as satellites in outer space or fiber-optic threads under water. Since hands-on repair is costly and sometimes virtually impossible, highly reliable IREDS with long operating lifetimes are essential. Great advances have been made in extending the operating lifetimes of IREDS, but less has been accomplished in modeling the failures.

The operating lifetime of an IRED is generally defined as the number of hours of use before the radiant power degrades to half of its initial value. Since an IRED operating lifetime can be greater than 10,000 hours, it is impractical to investigate the degradation process using normal operating conditions. For this reason, laboratory conditions that accelerate the radiant power degradation are used. Once the operating lifetime is determined for accelerated conditions, then a degradation model is employed to predict the operating lifetime under normal conditions.

This work investigates the use of the capacitance-voltage (C-V), current-voltage (I-V), and radiant power-current-voltage (P-I-V) diode characteristics as a means of

modeling the gradual radiant power degradation of silicon-doped gallium arsenide and gallium aluminum arsenide (GaAs:Si, GaAlAs:Si) IREDS. The procedure consists of measuring the initial characteristics, stressing with various operating current densities at room temperature, then periodically repeating the measurements. Control diodes that are not stressed are tested to determine the precision of the measuring apparatus and the "normal" variations in diode behavior. Once the data is acquired, the stressed and unstressed diode characteristics are compared to ascertain changes due to stressing. The parameters of interest are then presented as a function of time to determine if there is a relationship to the radiant power degradation.

CHAPTER II  
DIODE CHARACTERISTICS

A. Capacitance-Voltage

The space-charge capacitance (C) is defined as

$$C = \frac{dQ}{dV} \quad (1)$$

where

$dQ$  = the incremental increase in charge in the space-charge layer (coulombs)

$dV$  = the incremental change in applied voltage (volts)

The space-charge capacitance can be approximated by assuming the junction behaves like a parallel-plate capacitor [1, Page 40], or

$$C = \frac{A D K}{W} \quad (2)$$

where

A = the cross-sectional area of the junction ( $\text{cm}^2$ )

D = the dielectric constant of the material

K = the permittivity of free space

=  $8.854\text{E-}14$  farads/cm

W = the width of the junction (cm)

Adopting the convention where the width of the junction is in the x direction, Poisson's equation in one dimension is

$$\frac{d^2v}{dw^2} = \frac{-q N(W)}{D K} \quad (3)$$

where

$$\begin{aligned} q &= \text{the electronic charge} \\ &= 1.602\text{E-}19 \text{ coulombs} \end{aligned}$$

$N(W)$  = the doping concentration as a function of junction width (atoms/cm<sup>3</sup>)

The electric field (E) is

$$E = \frac{-dV}{dw} \quad (4)$$

Taking the derivative of (4) with respect to the junction width gives

$$\frac{dE}{dw} = \frac{-d^2v}{dw^2} \quad (5)$$

Substitution of (3) in (5) gives

$$\frac{dE}{dw} = \frac{q N(W)}{D K} \quad (6)$$

Solving for dE in (6) gives

$$dE = \frac{q N(W) dw}{D K} \quad (7)$$



Multiplying both sides of (7) by W gives

$$dE W = \frac{q N(W) dW^2}{D K} \quad (8)$$

Approximating (dE W) with dV [2, Page 171] gives

$$dV = \frac{q N(W) dW^2}{D K} \quad (9)$$

Solving (9) for N(W) gives

$$N(W) = \frac{D K}{q} \frac{dV}{dW^2} \quad (10)$$

Substitution of (2) in (10) gives

$$N(W) = \frac{1}{q D K A^2} \frac{1}{d(1/C^2)/dV} \quad (11)$$

Thus, if the area of the junction and the dielectric constant of the material are known, the appropriate differentiation of the capacitance-voltage characteristics will yield the doping concentration as a function of junction width. A FORTRAN program that implements (11) is included in APPENDIX I. Knowing the doping concentration is valuable because it provides information about current flow in the presence of electric fields. [2, Page 81]

#### B. Reverse Current-Voltage

The basic mechanism giving rise to a reverse current in a p-n junction diode is the generation of electron-hole

pairs somewhere in the semiconductor.[6, Page 173] When an electron-hole pair is generated within a diffusion length of the junction, the minority carrier will diffuse toward the junction and eventually be swept to the other side by the electric field. This reverse current component is called the reverse diffusion current ( $I_{Rd}$ ) and is given by

$$I_{Rd} = q A N_i^2 (D_n/N_a L_n + D_p/N_d L_p) \quad (12)$$

where

$N_i$  = the intrinsic carrier concentration ( $\text{cm}^{-3}$ )

$D_n$  = the electron diffusion coefficient ( $\text{cm}^2/\text{sec}$ )

$L_n$  = the electron diffusion length (cm)

$N_a$  = the acceptor concentration in the p-type region  
( $\text{cm}^{-3}$ )

$D_p$  = the hole diffusion coefficient ( $\text{cm}^2/\text{sec}$ )

$L_p$  = the hole diffusion length (cm)

$N_d$  = the donor concentration in the n-type region  
( $\text{cm}^{-3}$ )

If an electron-hole pair is generated within the space-charge region, both carriers will be swept by the electric field to the side of junction according to their polarities. This is known as the generation current ( $I_{Rg}$ ) and is given by

$$I_{Rg} = \frac{1}{2} q A N_i \frac{W}{T} \quad (13)$$

where

$T$  = the effective lifetime of a carrier within the reverse-biased space-charge region (sec)

A comparison of (12) and (13) reveals that  $I_{RD}$  is proportional to  $N_i^2$  whereas  $I_{RG}$  is proportional to  $N_i$ . Since  $N_i$  is a function of temperature [2, Page 76], the reverse current-voltage characteristics as a function of temperature should indicate which current component is dominant. Table 1 shows values of  $N_i$  and  $N_i^2$  for GaAs at various temperatures. The calculations supporting Table 1 are included in APPENDIX II. If the reverse current is due to diffusion, a rise in temperature from 25°C to 75°C should increase the current approximately 4000 times. Conversely, if the reverse current does not increase considerably, the generation current component is dominant.

TEMPERATURE (°C)	$N_i$ cm <sup>-3</sup>	$N_i^2$ cm <sup>-6</sup>	RATIO TO 25°C	
			$N_i$	$N_i^2$
25°C	2.3E+8	5.3E+16	1	1
75°C	1.5E+10	2.3E+20	65	4340
125°C	3.4E+11	1.2E+23	1478	2.3E+6
175°C	4.1E+12	1.7E+25	1.8E+4	3.2E+8

Table 1. Intrinsic Carrier Concentration for GaAs

### C. Forward Current-Voltage

In contrast to the reverse current, the basic mechanism giving rise to a forward current in a p-n junction diode is the recombination of electron-hole pairs in various regions of the semiconductor.[6, Page 182] When electrons are injected from the n-type region to the p-type region due to a forward bias, they become minority carriers and readily recombine with the majority carrier holes. Likewise, the holes as minority carriers in the n-type region recombine with the majority carrier electrons. This minority carrier injection constitutes a forward current component called the forward diffusion current ( $I_{Fd}$ ) and is given by

$$I_{Fd} = q A N_i^2 (D_n/N_a L_n + D_p/N_d L_p) [\exp(V/nV_t) - 1] \quad (14)$$

where

$V$  = the forward bias voltage (volts)

$n$  = the diffusion ideality factor

$V_t$  = the voltage equivalent of temperature (volts)

=  $\frac{\text{Temperature in degrees Kelvin}}{11,601}$

A comparison of (14) and (12) shows the similarities between the forward and reverse diffusion currents. Both components have the same magnitude ( $I_{d0}$ ) given by

$$I_{d0} = q A N_i^2 (D_n/N_a L_n + D_p/N_d L_p) \quad (15)$$

However, the forward diffusion current shows a strong dependence on voltage. In addition,  $I_{Fd}$  is a function of temperature through  $N_i^2$  and  $V_t$ .

Although the space-charge region diminishes in width with increasing forward bias, a portion of the carriers injected through the junction will recombine in the space-charge region. This forward current component is called the recombination current ( $I_{Fr}$ ) and is given by

$$I_{Fr} = \frac{1}{2} q A N_i \frac{W}{T} [\exp(V/mV_t) - 1] \quad (16)$$

where

$m$  = the recombination ideality factor

A comparison of (16) and (13) shows that both the generation current and the recombination current have the same magnitude ( $I_{r0}$ ) given by

$$I_{r0} = \frac{1}{2} q A N_i \frac{W}{T} \quad (17)$$

Just as in the forward diffusion current, the forward recombination current depends on forward bias and  $V_t$ , but the ideality factors are different. The diffusion current ideality factor is approximately 1 while the recombination ideality factor is about 2. The difference is due to the energy levels at which the electron-hole recombinations take place.[6,Page 134]

The total forward current is

$$I_F = I_{Fd} + I_{Fr} \quad (18)$$

Substitution of (14), (15), (16), and (17) in (18) gives

$$I_F = I_{d0}[\exp(V/nV_t) - 1] + I_{r0}[\exp(V/mV_t) - 1] \quad (19)$$

In general,  $I_{r0} \gg I_{d0}$ , therefore, the diffusion current can be neglected. However, at voltages above 1 volt, the diffusion current dominates because of its much sharper exponential rise. Thus, assuming  $V_t \ll V < 1$  volt, taking the logarithm of both sides of (19) after neglecting the diffusion current gives

$$\log I_F = \log I_{r0} + \frac{\log e}{mV_t} V \quad (20)$$

A plot of  $\log I_F$  vs  $V$  should yield a straight line with the following parameters:

$$\text{slope} = \frac{\log e}{mV_t} \quad (21)$$

$$\text{y-intercept} = \log I_{r0} \quad (22)$$

From this discussion, it would appear that at voltages above 1 volt, the recombination current could be neglected and the diffusion current could be found in a manner similar to (21), but two major factors contribute to the failure of this approach. First, every diode exhibits a series resistance due to the length that the holes and electrons

$I_F$  = the forward DC current (amperes)

$V$  = the forward voltage (volts)

Using the forward voltage values measured with a FLUKE Model 8000A Digital Multimeter, the following values of  $P_d$  were calculated:

IRE D	$P_d$ (100mA) (W)	$P_d$ (200mA) (W)
Honeywell SE5450	.138	.303
Honeywell SE3470	.146	.319
TRW OP131	.151	.337
TRW OP233	.151	.340

Substitution of (5.2), (5.3),  $P_d$ , and  $T_a = 27^\circ\text{C}$  in (5.1) gives the following values of  $T_j$ :

IRE D	$T_j$ (100mA) ( $^\circ\text{C}$ )	$T_j$ (200mA) ( $^\circ\text{C}$ )
Honeywell SE5450	52	83
Honeywell SE3470	54	86
TRW OP131	55	89
TRW OP233	55	90

END

JAN.

1988

DTIC